General Disclaimer

One or more of the Following Statements may affect this Document

- This document has been reproduced from the best copy furnished by the organizational source. It is being released in the interest of making available as much information as possible.

- This document may contain data, which exceeds the sheet parameters. It was furnished in this condition by the organizational source and is the best copy available.

- This document may contain tone-on-tone or color graphs, charts and/or pictures, which have been reproduced in black and white.

- This document is paginated as submitted by the original source.

- Portions of this document are not fully legible due to the historical nature of some of the material. However, it is the best reproduction available from the original submission.

LA-3981

AUTHOR'S COPY

LOS ALAMOS SCIENTIFIC LABORATORY
of the
University of California
LOS ALAMOS • NEW MEXICO

The Manufacture and Properties of an Extruded, Resin-Bonded Graphite, CMF-13 Lot AAQ1

UNITED STATES
ATOMIC ENERGY COMMISSION
CONTRACT W-7405-ENG. 36

LA-3981
UC-25, METALS, CERAMICS,
AND MATERIALS
TID-4500

LOS ALAMOS SCIENTIFIC LABORATORY
of the
University of California
LOS ALAMOS • NEW MEXICO

Report written: July 1968

Report distributed: October 31, 1968

The Manufacture and Properties of an Extruded, Resin-Bonded Graphite, CMF-13 Lot AAQ1

by

Morton C. Smith

THE MANUFACTURE AND PROPERTIES OF AN EXTRUDED, RESIN-BONDED GRAPHITE, CMF-13 LOT AAQ1

by

Morton C. Smith

ABSTRACT

CMF-13 Lot AAQ1 is a relatively large sample of an extruded, resin-bonded graphite. It was manufactured from commercial raw materials, which are fully characterized, and using standard procedures, which are described in detail. The principal physical and mechanical properties of the finished graphite are listed, in most cases as functions of temperature.

I. INTRODUCTION

Most commercial graphites are manufactured from mixtures of petroleum coke, carbon black, and coal-tar pitch. For special purposes, however, when the economies of a particular situation justify it, other raw materials are sometimes substituted. One occasionally useful modification of the basic graphite formula is the substitution of graphite flour for petroleum coke, principally to reduce shrinkage of the formed material during baking and graphitizing. Another is replacement of the pitch binder with a thermosetting resin, which makes possible forming at room temperature to close dimensional tolerances and avoids slumping of the formed body during subsequent heat treatment.

A graphite incorporating both of these modifications has been developed at Los Alamos Scientific Laboratory, principally by Group CMB-6, and used in a variety of critical applications, for example, as the matrix to contain pyrocarbon-coated UC_2 fuel particles in fuel elements for the UHTREX nuclear reactor.[1] A common formulation of this graphite, by weight, is: 85 parts graphite flour, 15 parts carbon black, and 27 parts furfuryl alcohol resin catalyzed with maleic anhydride.

Several of the properties of such a graphite have been examined in some detail. Most of the measurements made, however, have been on fuel elements, the properties of which are affected by the presence within the graphite of a variable proportion of relatively coarse fuel particles and by the fact that, to avoid thermal degradation of these particles, the material has been graphitized at an abnormally low temperature.

A large sample of a graphite of this type, identified as CMF-13 Lot AAQ1, has therefore been made to serve the following purposes:

1. To demonstrate the state of the art of graphite manufacturing in LASL Group CMF-13, and particularly the quality and uniformity possible in such a graphite when each step of its manufacture is controlled to the degree that has become possible in Group CMF-13;
2. To determine the properties and examine the be-

havior of a good graphite of this type free of dispersed fuel particles and in the condition in which it would exist after normal graphitization or after service at high temperature;

3. To establish a reliable base line against which to compare the properties of other experimental graphites in which filler materials, binder, and manufacturing procedures have been varied systematically.

AAQ1 graphite has been manufactured from commercial raw materials, in standard proportions, using common commercial equipment and manufacturing processes. The raw materials used have been characterized in detail, complete records have been kept at every stage of manufacture, and the properties of the finished graphite have been examined in depth.

II. RAW MATERIALS

AAQ1 graphite was produced from a raw-materials mix that contained 85 parts by weight of Great Lakes 1008-S graphite flour, 15 parts by weight of Thermax carbon black, and 27 parts by weight of Varcum 8251 furyl alcohol resin. The resin contained 4% by weight of maleic anhydride as a polymerization catalyst, which is included in the 27 parts of binder listed above.

A. Graphite Flour

Grade 1008-S is a high-purity flour manufactured by Great Lakes Carbon Corporation. It is produced from a special graphite made from a relatively nonacicular petroleum coke bonded with coal-tar pitch, and is ground to a LASL specification on screen-size analysis. The material used to manufacture AAQ1 graphite was taken from a larger lot of 1008-S flour purchased by LASL Group CMB-6 and identified by them as "M2" graphite flour. It was reblended and identified by Group CMF-13 as "Lot G-13" flour.

The characteristics of this graphite flour are summarized in Table I. The photomicrographs of Fig. 1 give an impression of the shapes and internal structures of the particles composing it. They represent--at different magnifications--two areas on a vertical section through a sedimentation column of flour particles permitted to settle freely in an epoxy resin. The resin was caused to polymerize before settling was complete, "freezing" the par-

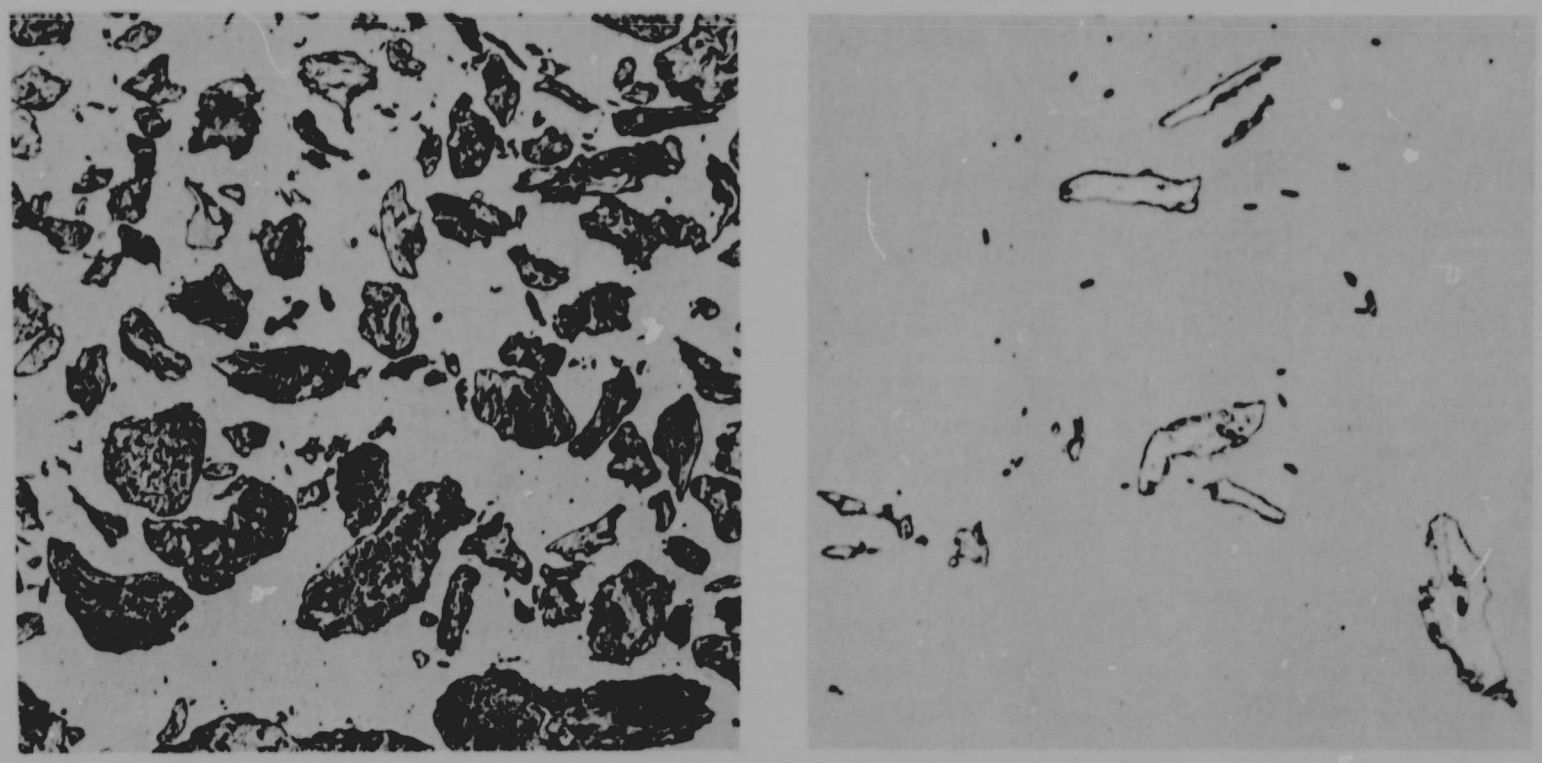

a. b.

Fig. 1. Vertical sections through column of Lot G-13 graphite flour settling in epoxy resin. Hydrogen-ion etch; bright-field illumination. (a) Near bottom of column. 100X. (b) Fines near top of column. 500X.

TABLE I

SAMPLE DATA ON LOT G-13 GRAPHITE FLOUR

Screen Analysis (U. S. Std.), Wt. %:

	+20 mesh	0.0%
-20	+35 mesh	0.1%
-35	+70 mesh	0.7%
-70	+100 mesh	4.2%
-100	+140 mesh	11.4%
-140	+200 mesh	24.4%
	-200 mesh	58.9%

Micromerograph Analysis, Wt. %:

> 200 μ		1.9%
200 >	100 μ	23.2%
100 >	70 μ	19.0%
70 >	44 μ	22.0%
44 >	25 μ	14.0%
25 >	10 μ	10.0%
10 >	5 μ	6.5%
5 >	2 μ	2.9%
<	2 μ	0.4%

Micromerograph Sample Statistics:

$\hat{\mu}_{x3} = 4.041$

$\hat{\sigma}_x^2 = 1.646$

$\hat{\mu}_x = -0.597$

$\bar{d}_3 = 123.2\ \mu$

$s^2_{d_3} = 56,089.\ \mu^2$

$\bar{d} = 1.192\ \mu$

$s^2_d = 5.249\ \mu^2$

$CV_d = 1.922$

Crystalline Parameters:

$L_c = 551$ Å

$d_{002} = 3.360$ Å

Helium Density: 2.199 g/cm^3

Specific Surface:

Measured	3.685 m^2/g
Calculated	0.114 m^2/g
Fuzziness ratio	49.9

Chemical Analysis:

H_2O	220 ppm
Ash	220 ppm
Fe	40 ppm
S	10 ppm
Si	100 ppm
Ca	30 ppm
V	10 ppm
Ni	10 ppm
Mg	1 ppm
B	< 1 ppm

(All other common impurities below detection limits of semiquantitative spectrochemical analysis.)

---

ticles in place in a vertical distribution of sizes and shapes. Most of the particles have well-graphitized, lamellar internal structures. The coarser ones tend to have surface-connected internal porosity, which has been entered by the epoxy resin. The finer particles are generally free of visible internal pores presumably because, in grinding to this size range, fracture occurred preferentially through such voids. The coarser particles, near the bottom of the settling column, are not particularly acicular in cross section. There is an evident tendency to become so in the medium size range, and the fine particles are usually quite acicular in section. A description of this graphite flour as "nonacicular" simply means that it is less acicular than many other graphite flours.

Helium density and specific surface area of G-13 flour are both relatively high, again suggesting that most of the internal porosity of individual particles is surface-connected. Its "fuzziness ratio"--which is the ratio of specific surface area measured by gas adsorption to that calculated from Micromerograph sample statistics assuming all particles to be smooth-shelled spheres--is extremely high. Particle surfaces are evidently much less smooth than they appear to be in Fig. 1, and a large increment of surface area not apparent in a photomicrograph is probably accounted for by very narrow interlamellar separations extending inward from particle surfaces.

Micromerograph size-analysis data agree reasonably well with the screen analysis. As seems usually to be true of commercial coke and graphite flours, these data are only fairly well approximated by the general log-

normal function. (This is probably a joint result of the highly developed cleavage systems available in certain particle-size ranges and some peculiarity of the grinding action in the Raymond mills generally used to grind cokes and graphites.) Of particular interest in the sample statistics derived from these data is the relatively high value of CV_d, the coefficient of variation of a linear particle dimension, d. According to the Lewis-Goldman mixing model, this indicates that the flour should pack to relatively high density in a forming operation.

B. Carbon Black

The carbon black used as part of the filler in manufacturing AAQ1 graphite was "regular" Thermax, a furnace black manufactured by Thermatomic Carbon Co. It was purchased directly from the manufacturer, and was identified by CMF-13 as "Lot TP-3" carbon black.

As is illustrated by the electron micrograph (Fig. 2), individual Thermax particles are smooth-shelled and nearly spherical. Many of them, however, appear as aggregates, which are not broken up by any deagglomeration technique so far tried here. (These may, in fact, often represent intergrowths of particles, as is frequently suggested by their shapes.) Accordingly, two sets of optical size-analysis data were collected, one representing individual spherical particles including those composing aggregates, and the other representing agglomerates including isolated individual spheroids as well as clusters of these. Both sets of data are plotted in Fig. 3 and sample statistics for both are listed in Table II. The agglomerate count gave a poorly defined distribution curve,

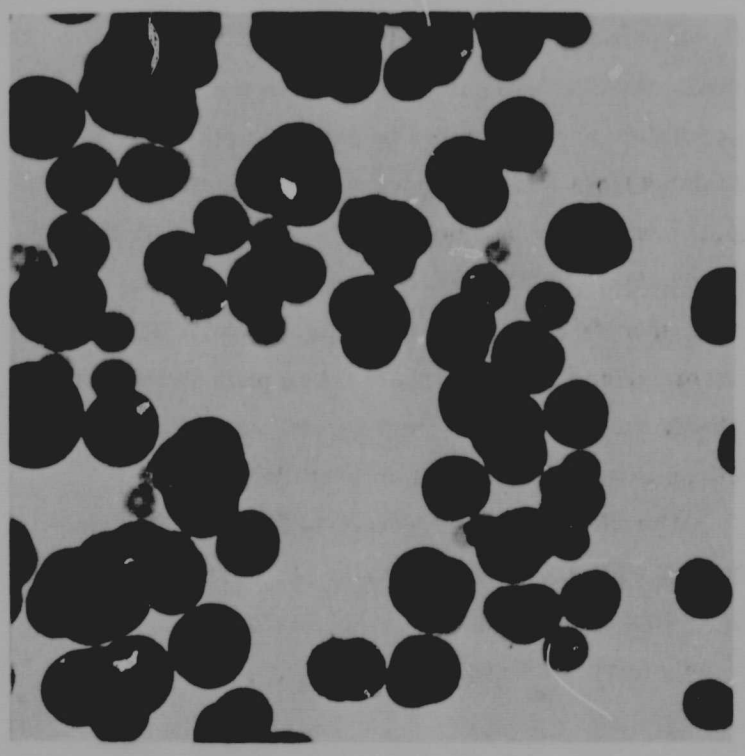

Fig. 2. Thermax carbon black, Lot TP-3. 20,000 X.

TABLE II

SAMPLE DATA ON THERMAX CARBON BLACK, LOT TP-3

Crystalline Parameters:

L_c = 17.4 Å

d_{002} = 3.47 Å

Amorphous Carbon ≅ 47%

Unassociated Layers = 13%

Helium Density: 1.880 g/cm^2

Specific Surface:

Measured = 8.9 m^2/g

Calculated = 7.43 m^2/g

Fuzziness Ratio = 1.198

Size-Distribution Statistics:

	Particles	Agglomerates
$\bar{d}$	0.328 μ	0.538 μ
s_d^2	0.014 μ^2	0.066 μ^2
s_d	0.118 μ	0.257 μ
g_d	1.049 μ^3	1.150 μ^3
M_d	0.295 μ	0.323 μ
N	1716	403

$\bar{d}_A/\bar{d}$ = 1.64

N/N_A = 4.23

Chemical Analysis:

H_2O	= 0.03%	Si	= 900 ppm
Ash	= 0.23%	Ca	= 30 ppm
S	= 0.04%	Mg	= 15 ppm
Fe	= 20 ppm	B	< 1 ppm

(All other common impurities below detection limits of semiquantitative spectrochemical analysis.)

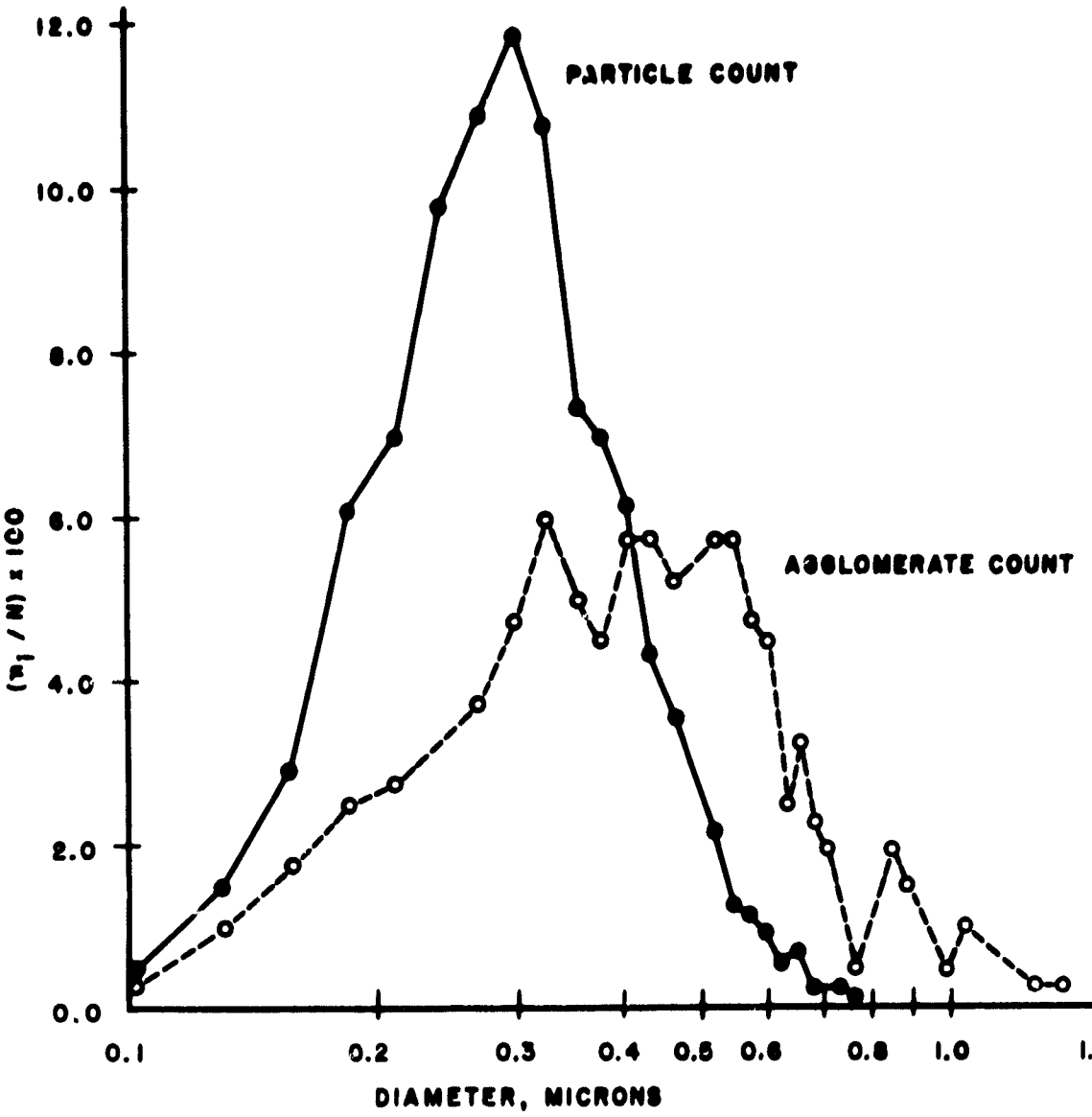

Fig. 3. Particle and agglomerate counts for Thermax carbon black, Lot TP-3.

indicating that sample size (403 individuals) was not large enough. The particle count (1716 particles) produced a well-defined distribution curve.

Agreement between specific surfaces measured by gas adsorption and calculated from optical-count sample statistics is quite good, giving an unusually low fuzziness ratio and indicating that in this case the assumption of smooth-shelled spherical particles was reasonable. The low fuzziness ratio also confirms the relatively low helium-density value in indicating that most of the internal porosity of the Thermax particles is not surface-connected.

The calculated diameter of monosize spheres which would have specific surface area equal to that measured by gas adsorption is 0.359 μ, in good agreement with the average particle diameter of 0.328 μ determined from the optical count. The fact that the calculated value is slightly higher than the measured one would be expected because the size distribution has nonzero variance and is positively skewed.

Small samples of Lot TP-3 Thermax, contained in graphite crucibles, have been heat-treated for 30 min at 2800°C, and then examined by electron microscopy and x-ray diffraction. The external shapes of individual particles were observed in general to have changed from spherical to polyhedral, usually with quite well-developed facets. Their average crystallite size, L_c, increased markedly, from 17.4 Å to 225 Å, and their average interplanar spacing, d_{002}, decreased significantly, from 3.47 Å to 3.378 Å. The degree of graphitization which

these changes represent was unexpectedly large for a carbon black.

C. Furfuryl Alcohol Resin

Varcum 8251 is a dark, polymeric, liquid resin manufactured by the Varcum Chemical Division of Reichold Chemicals, Inc., by polymerization of furfuryl alcohol. Its density is 1.2 g/ml and its viscosity at 25°C is approximately 250 cp.

The molecular distribution of the Varcum used to manufacture AAQ1 graphite was determined at room temperature using a Waters Model 200 gel permeation chromatograph equipped with three elution columns in series. Maximum pore diameters of the polystyrene gels with which the columns were packed were, respectively, 8×10^3 Å, 250 Å, and 45 Å. Resin samples were injected as 1.0% by weight solutions in tetrahydrofuran, with injection time of 30 sec. Flow rate of the tetrahydrofuran solvent was 1 ml/min. The column system was calibrated with respect to molecular weight by determining the elution positions of a series of samples of polyethylene and polypropylene glycols having narrow molecular weight distributions and of the furfuryl alcohol monomer, dimer, and trimer. Fig. 4 is the chromatogram produced, with Δn (relative refractive index, representing solute concentration) plotted against approximate molecular weight of the solute.

Polymerization of furfuryl alcohol produces several chemical species within each molecular size range. Therefore each point on the chromatogram represents total detector response to all species emerging at that elution volume, and individual species cannot in general be identified. However, peaks representing the monomer, dimer, and trimer are resolved at molecular weights of about 100, 200, and 300, respectively. The distribution shown in Fig. 4 is very similar to those of furfuryl alcohol resins of similar viscosity prepared in CMF-13 using either maleic anhydride or phosphoric acid as the polymerization catalyst. However, the Varcum resin has a distinctly higher content of monomer and shows a greater

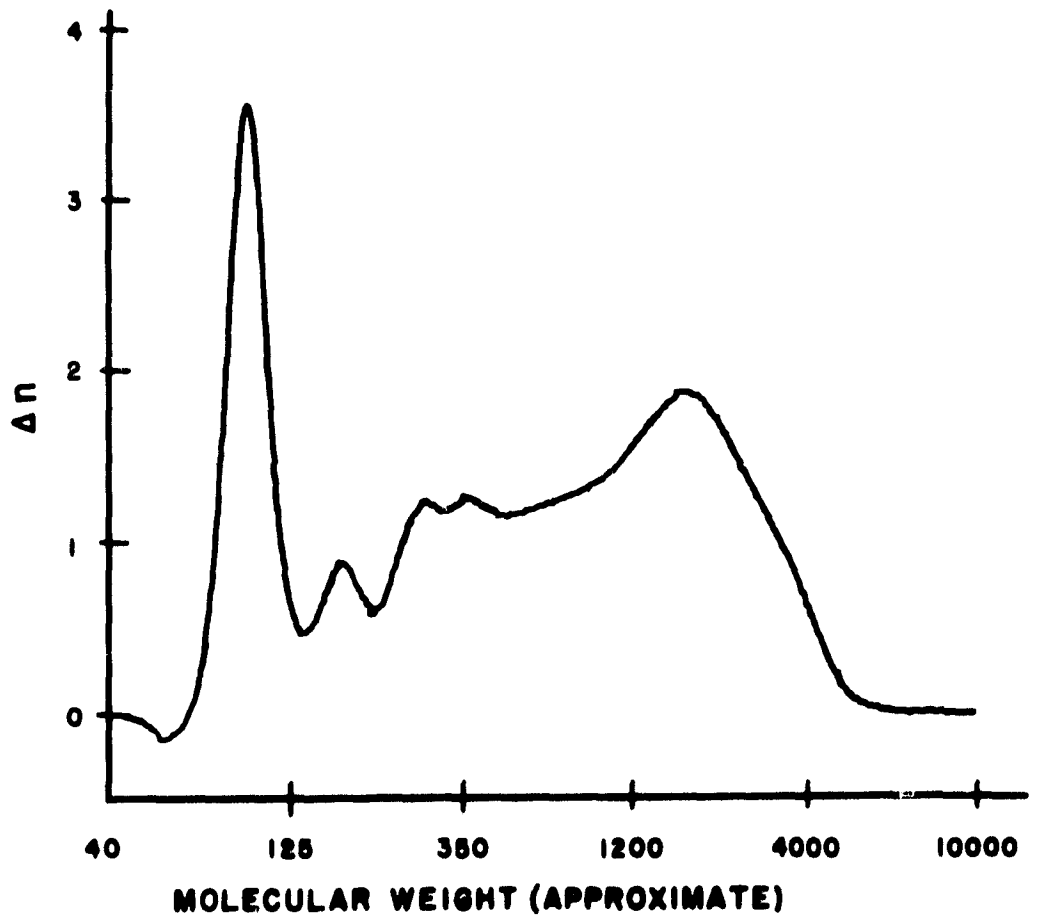

Fig. 4. Gel permeation chromatogram of Varcum 8251 resin used to manufacture Lot AAQ1 graphite.

degree of conversion to the higher molecular-weight products. This is apparently the result of a manufacturing process in which viscosity of the partially polymerized resin is reduced by additions of the monomer. (Other lots of Varcum 8251 investigated have differed from this one, principally in the intermediate and high molecular-weight regions.)

This lot of Varcum resin has also been characterized by differential thermal analysis, which is not sensitive to small changes in resin structure but is informative concerning the overall chemical processes that may be expected to occur during curing and baking of a graphite made from it. This was done in a duPont Model 900 differential thermal analyzer operated with a dead-air sample environment and a ΔT sensitivity of 0.02 mv (0.5°C) in. Sample weight was 50 mg, the sample consisting of 60% by weight of 125 to 149 μ graphite flour and 40% catalyzed resin, the latter including maleic anhydride curing catalyst in the proportion of 5% of the weight of resin. The reference sample was 30 mg of the same graphite flour. The sample was weighed into a 4-mm-dia sample tube and tamped to a depth of 5 mm with a steel rod. Heating rate was 30°C/min. from ambient temperature to 500°C. A small exotherm occurred at 115 to 130°C, an endotherm at 130 to 145°C, a large exotherm at 165 to 185°C, and a broad exotherm around 390°C. The differential thermal analysis curve was very similar to those of a series of CMF-13 experimental resins prepared using maleic anhydride as the catalyst, many of which differed widely from the Varcum resin in molecular distribution. The principal difference was reduced intensity of the exotherm in the 180°C region in the case of the more viscous experimental resins, in which the higher molecular-weight species predominated.

D. Maleic Anhydride

In the manufacture of AAQ1 graphite, the polymerization catalyst used was maleic anhydride in the proportion of 4% of the weight of Varcum resin binder. This catalyst was dissolved in acetone in the proportion 7.56 g maleic anhydride to 10 ml acetone, and the solution was mechanically stirred into the resin for 15 min at room temperature.

Use of acetone in this way is not standard in the manufacture of resin-bonded graphites. However, it assists in distributing the catalyst throughout the resin, to produce more uniform polymerization, and also reduces viscosity of the binder, facilitating subsequent mixing with the filler. The acetone is believed to have been completely removed from the mix by evaporation before the mix was extruded.

III. GRAPHITE MANUFACTURE

A. Mixing

The mix used for the manufacture of AAQ1 graphite was prepared in six batches, each containing 1400 g of filler material. The dry graphite flour and carbon black were weighed individually, hand-stirred together briefly, then mixed for 15 min in an 8-qt Patterson-Kelly twin-shell blender equipped with an intensifier bar. The filler mix was removed from the blender, the catalyzed binder was hand-kneaded into it for 10 min, and the "wet" mix was returned to the blender. Again using the intensifier bar, the mix was blended for 15 min, with interruptions after 5 min and 10 min of blending to scrape adhering material from the interior of the blender. After blending, the six batches were bottled individually and stored overnight in a refrigerator. The next morning, after the mix had warmed again to room temperature, the six batches were combined into one large batch. This was hand-stirred, then passed five times through a Hobart meat grinder equipped with a chopping plate having 0.125-in. dia holes.

The chopped mix, at a temperature of 42°C, was loaded into the materials chamber of a 40-ton Loomis tiltable hydraulic extrusion press (operated in the horizontal position), in batches large enough to make about 100 in. of 0.5-in.-dia extruded rod. The chamber was evacuated to a residual pressure of about 500 μ, which was maintained for 1 min. Then the ram was advanced to develop pressure of 3200 psi, which was maintained for 1 min. Finally, pressure was increased

to about 5000 psi and the mix was extruded as 0.5-in.-dia rod at 12 to 16 in. min. Because of cooling while the early batches were extruded, the later batches were extruded at somewhat lower temperatures, higher pressures, and lower rates.

Rods produced at this stage were crumbled, hand-stirred into one large batch, and chopped by one pass through the meat grinder. Enough material to fill the chamber of the press was then chopped again just before it was loaded into the press, and was extruded again under the conditions listed above. When the entire lot had been re-extruded, the rods were again crumbled, hand-stirred into one batch, and chopped again.

Subsequent to twin-shell blending, then, the raw-materials mix was further mixed by chopping it five times, extruding it, chopping it twice, extruding it again, and chopping it once. Finally it was separated into batches large enough to produce one extrusion each, and each batch was chopped once more just before it was loaded into the press for final extrusion.

B. Extrusion

During the last chopping operation, mix temperature was adjusted to 42°C. The mix was then loaded into the materials chamber of the extrusion press, which was held at 50°C by electrical-resistance strip heaters. The evacuation and pressure cycle used were those outlined above except that final extrusion pressure was carefully maintained at 7600 psi. Extrusion conditions are summarized in Table III.

Each extrusion was about 0.501-in.-dia and 100-in. long. It was caught as it left the die in a split copper tube lubricated with flake graphite. The first 7 to 16 in. of each extrusion were cropped off, and the rest of the extrusion was cut into 10-in. long rods which were numbered consecutively on their leading ends. Material cropped from extrusions 1 through 14 was crumbled, hand-stirred together with material reclaimed from chopper cleanups, etc., chopped twice, and extruded under the above conditions to produce extrusions 15, 16, and 17.

The extrusion system used was a materials chamber 2 in. dia and 15 in. long followed by a simple breaker-plate and die which gave a 16 to 1 extrusion ratio. The breaker-plate was a hardened steel cylinder 2.625-in. dia and 1.375-in. long containing six 0.563-in.-dia holes equally spaced on a 1.5-in.-dia circle. Both ends of each hole were countersunk sufficiently to form sharp edges between holes. Conical protrusions on the center line on both sides of the breaker-plate increased pressure on the mix locally and maintained a smooth material flow into the die. The die had a 60° included-angle lead-in tapering from 1.75 to 0.500 in. dia. The land of the 0.500-in.-dia die opening was 2.168 in. long and was ground to 8 μ in. rms. The die was heated only by conduction from the materials chamber and by flow of material through it. However, after the first few passes -- which were part of the mixing process --the temperature of the die body and materials chamber were uniform.

C. Curing

The numbered 0.50-in.-dia, 10-in. long, green extruded rods were laid horizontally in grooved graphite blocks which were loaded into trays and covered with carbon black. Each tray was covered with aluminum foil, and all trays were loaded together into a Model V23-SD Despatch electric recirculating air oven. In an air atmosphere, they were heated to 200°C over a period of 69 hr in the following cycle: heating from 20 to 45°C at 3.13°/hr; holding at 45°C for 10 hr; heating from 45 to 90°C at 5°/hr; heating from 90 to 138°C at 2°/hr; heating from 138 to 200°C at 5.17°/hr; holding at 200°C for 8 hr; furnace-cooling to room temperature.

D. Baking

The cured rods were wiped free of adhering carbon black and inserted horizontally into 0.625-in.-dia holes drilled in a 5.75-in.-dia commercial graphite rod 12 in. long. This was loaded into a Model 290-71 Marshall horizontal electric tube furnace. The furnace chamber was evacuated to a residual pressure of 100 μ or less, then heated to 900°C over a period of 41 hr in the following cycle: heating from 20 to 450°C at 19.55°/hr; heating from 450 to 900°C at 23.68°/hr; holding at 900°C for 2 hr;

TABLE III

FINAL EXTRUSION CONDITIONS FOR GRAPHITE AAQ1

Ext. Batch No.	Vacuum μ	Holding Pressure psi	Extrusion Pressure Max. psi	Extrusion Pressure Min. psi	Speed in./min	Temp. °C	Rod No.	Green Rod Dia. in.	Lead End Discard in.
1	500	3200	7000	6400	147	52	1 to 10	0.502	8
2	500	3200	7600	7000	147	42	11 to 18	0.501	13
3	500	3200	7600	7000	156	41	19 to 26	0.501	9
4	500	3200	7600	7000	156	42	27 to 33	0.501	16
5	500	3200	7600	7000	160	42	34 to 41	0.501	9
6	500	3200	7600	7000	164	42	42 to 50	0.501	9
7	550	3200	7600	7000	160	42	51 to 59	0.501	10
8	650	3200	7600	7000	150	42	60 to 68	0.501	8
9	600	3200	7600	7000	153	42	69 to 77	0.501	10
10	650	3200	7600	7000	156	42	78 to 86	0.501	11
11[a]	650	3200	7600	7000	171	42	87 to 94	0.501	23
12	650	3200	7600	6800	167	42	95 to 103	0.501	10
13	600	3200	7600	6400	171	42	104 to 112	0.501	14
14	1000	3200	7600	---	167	42	113 to 121	0.501	7
15[b]	600	3200	7600	7300	133	40	122 to 129	0.501	11
16[b]	600	3200	7600	7600	100	38	130 to 138	0.501	8
17[b]	600	3200	8900	8300	176	38	139 to 147	0.501	11

(a) Ten inches of rod were extruded before pressure held; leading-end discard was increased to allow this material to be discarded.

(b) Extrusion batches 15, 16, and 17 were made from leading-end discards and other material reclaimed from earlier operations, which were combined, chopped twice, and extruded. They therefore differ slightly from earlier extrusion batches.

furnace-cooling to nearly room temperature in about 24 hr.

Processing of all rods in Lot AAQ1 required five baking runs. So far as could be determined, baking conditions were identical in all runs. Rods baked in each run are identified in Table IV. Rod No. 1 was subsequently damaged in handling, and was discarded.

E. Graphitizing

Baked rods were cut to a standard length of 9.25 in., the maximum that could be contained in the resistively-heated Model 550-C Brew furnace used for graphitizing. They were loaded vertically into the furnace chamber, which was evacuated and refilled with helium twice. Then, maintaining a very slow flow of helium through the furnace, the rods were heated at a nearly constant rate to 2830°C over a period of 6 hr, and furnace-cooled to nearly room temperature in about 3 hr. Rods numbered 2 through 77 were graphitized together in one run, and rods 78 through 147 in a second run essentially identical with the first.

TABLE IV

IDENTIFICATION NUMBERS OF RODS INCLUDED IN EACH BAKING RUN

Run No. 86	Run No. 87	Run No. 88	Run No. 89	Run No. 90
1	27 to 29	42 to 49	30 to 41	117 to 1
2 to 26	50 to 76	77 to 92	92 to 98	
		99 to 105	106 to 116	

IV. STRUCTURE

A. Electron and Optical Microstructure

The microstructure of a typical longitudinal section through a finished AAQ1 graphite rod is shown in Fig. 5 at 100X magnification. There is some evidence of a tendency for the larger and more acicular filler particles to assume orientations in which their longest dimensions are approximately parallel to the extrusion axis. The epoxy resin used to impregnate and mount such specimens was found to penetrate the graphite only to a very limited depth, indicating a low proportion of connected porosity.

Another typical section is shown in Fig. 6, with a slightly different etch and at 10,000X. The relatively small, approximately equiaxed areas represent particles of carbon black. From comparison with Fig. 2, these

Fig. 5. Longitudinal section through AAQ1 graphite extrusion. Extrusion axis is vertical. Hydrogen-ion etch; bright-field illumination; 100X.

appear in many cases to have developed somewhat angular outlines, suggesting that they may have graphitized to some degree during the graphitizing heat-treatment of the rods. The presence of these particles identifies regions occupied by the graphitized binder residue between larger particles of graphite flour having obviously lamellar internal structures. Mixing of raw materials was evidently good, and this and most other sections examined appeared to be dense, well bonded, and essentially free of voids and cracks. However, a few small voids and clusters of voids were encountered. Figure 7 shows the longest stringer of voids observed. A few c-face cracks were also found, one of which is shown in Fig. 8.

The most serious type of defect noted was that illustrated in Fig. 9. This is a series of connected cracks, extending through the binder residue between filler particles, and located just below and approximately parallel to the cylindrical surface of the extrusion. These cracks are believed to have formed as a result of an elastic springing apart of filler particles when, as the extrusion emerged from the die, the radial compressive stresses developed by the die wall were relieved and the rod was permitted to expand. Although not common, cracks of this type were found in several of the AAQ1 extrusions.

B. Microradiography

Thin longitudinal and transverse slices of AAQ1 graphite, cut from Rod 22, were vacuum-impregnated with sulfur and microradiographed (by LASL Group GMX-1) at section thicknesses of about 0.005, 0.010, and 0.020 in. Because sulfur is more opaque to x-rays than is carbon, voids intruded by sulfur appear as light areas in the radiograph and as dark areas on prints made

Fig. 6. Electron micrograph of AAQ1 graphite. Xenon-ion etch; 10,000 X.

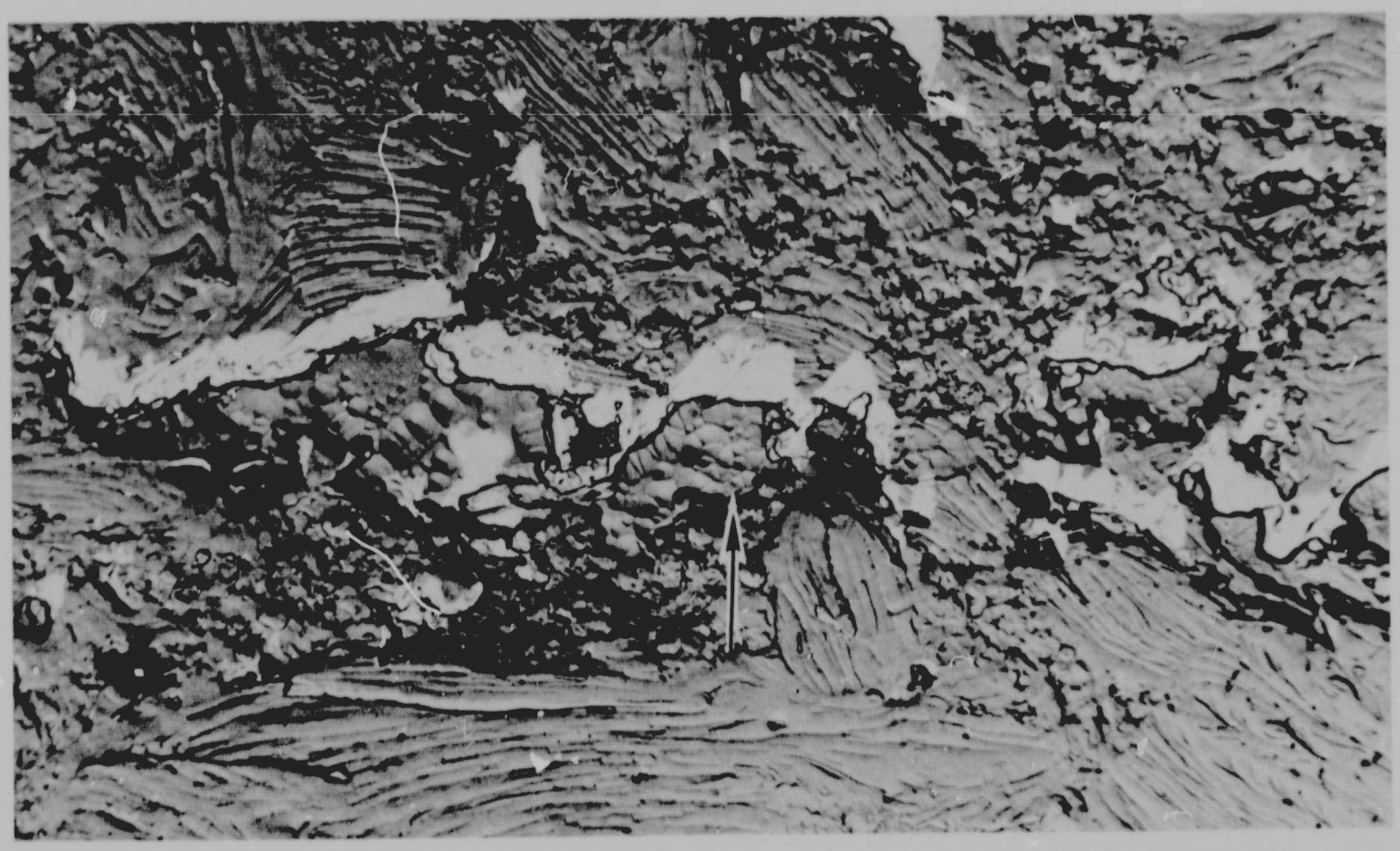

Fig. 7. Void stringer in AAQ1 graphite. Xenon-ion etch; 5000 X. In this section the voids have been filled with an epoxy resin which has etched in a distinctive conchoidal pattern. The arrow indicates one such void.

Fig. 8. C-face crack in AAQ1 graphite. Xenon-ion etch; 5000X. The crack has been filled with epoxy resin, and extends almost horizontally across the picture, at the edge of a large particle of graphite flour. A void cluster appears below it.

Fig. 9. Transverse section through AAQ1 graphite extrusion, showing epoxy-filled, circumferential, interparticle crack. Irregular dark spots are holes, believed to be polishing artifacts. Unetched; bright-field illumination; 150X.

from it.

Figure 10 is a pair of prints typical of such microradiographs, enlarged optically to about 5X. The concentration of light areas near the cylinder axis represents a relatively large region of low porosity around the center of the extruded section, which absorbed very little sulfur. This is believed to be associated with merging in the die of six separate streams of material emerging from the six holes in the breaker-plate. A faint herringbone pattern is visible near the edges of the longitudinal section, representing an alignment of voids between flake-like filler particles which, in this region, tend to assume orientations in which they are inclined at about 30° to the extrusion axis. A tendency toward a tangential arrangement of these particles is evident in the transverse section.

a.

b.

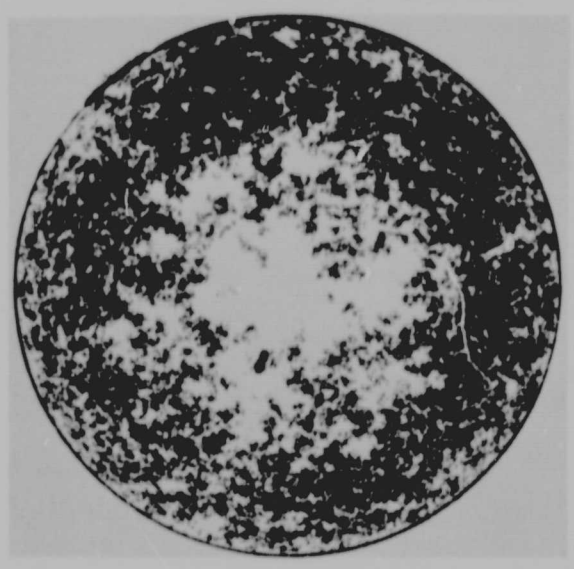

Fig. 10. Microgradiographs of sulfur-impregnated longitudinal (a) and transverse (b) slices of AAQ1 graphite, each about 0.020-in. thick. Tungsten continuous radiation at 15 kv; Kodak High-Resolution Plate; subsequent optical enlargement to about 5 X.

C. X-Ray Diffraction

Average crystallite thickness, L_c, and average interplanar spacing, d_{002}, of AAQ1 graphite were 405 Å and 3.362 Å, respectively. These parameters represent a well-graphitized material although, because of dilution of the graphite flour by the less well-graphitized carbon black and binder residue, L_c is actually smaller and d_{002} larger than for the original flour.

Preferred orientations were analyzed for samples taken from both ends of each of four different rods. Results are listed in Table V, where σ_{ox}/σ_{oz} is the Bacon anisotropy factor and M is the exponent of the sine function, $I(\Phi) = I_o \sin^M \Phi$, which best describes the change in concentration of basal planes with angle relative to the extrusion axis. The average Bacon factor and M value represent a moderately high degree of preferred orientation of the order normally found in small-diameter extruded graphite rod. Very little difference in texture was observed within individual rods or from rod to rod.

TABLE V

PREFERRED ORIENTATIONS OF AAQ1 GRAPHITE RODS

Rod No.	Rod End	M	σ_{ox}/σ_{oz}
AAQ1-3	Leading	1.59	1.34
AAQ1-3	Trailing	1.70	1.38
AAQ1-40	Leading	1.73	1.37
AAQ1-40	Trailing	1.70	1.34
AAQ1-98	Leading	1.55	1.34
AAQ1-98	Trailing	1.57	1.34
AAQ1-130	Leading	1.69	1.39
AAQ1-130	Trailing	1.61	1.36
Average		1.64	1.36

V. CHEMICAL COMPOSITION

Semiquantitative spectrochemical analysis of samples of AAQ1 graphite (by LASL Group CMB-1) indicating the presence of the following concentrations of common impurities:

Ash	<	300 ppm
Fe	=	30 ppm
Si	=	30 ppm
B	<	1 ppm .

All other common impurities were present in concentrations below the detection limits of the analytical method used.

The raw materials used to manufacture this graphite were quite pure, and composition changes during mixing, forming, and heat-treating were small. No significant contamination of the material occurred during processing, and the general reduction in impurity levels expected to occur during heat-treatment was realized.

TABLE VI

POROSITY DISTRIBUTIONS OF AAQ1 GRAPHITE

Sample No.	Total Porosity %	Porosity Accessible to 2600 psi Hg %	$\bar{x}_3$	s^2_{x3}	s_{x3}
AAQ1-6	16.0	3.2	-0.75	0.63	0.96
AAQ1-19	15.8	2.9	-0.86	0.57	0.88
AAQ1-22	15.8	3.0	-0.75	0.57	0.31
AAQ1-26	15.9	3.2	-0.77	0.66	1.25
AAQ1-47	16.0	3.2	-0.82	0.46	0.41
AAQ1-55	15.9	3.1	-0.82	0.56	0.70
AAQ1-69	15.7	3.0	-0.83	0.57	0.77
AAQ1-77	16.2	3.6	-0.78	0.62	0.83
AAQ1-98	15.9	3.1	--	--	--
AAQ1-113	16.1	3.7	-0.6	0.54	0.14
AAQ1-122	15.9	3.4	-0.73	0.66	1.01
AAQ1-133	15.5	3.0	-0.74	0.39	0.80
Average	15.9	3.1	-0.77	0.57	0.64
σ	0.2	0.2	0.08	0.08	0.3

VI. PROPERTIES

A. Density

Bulk density of each rod of AAQ1 graphite was determined individually by weighing and measuring it. Weighing to the nearest 0.001 g was on an analytical balance. Length measurements to the nearest 0.001 in. were made in a jig equipped with a dial micrometer, and diameters were measured similarly, to the nearest 0.000,1 in. Measurements of 10 rods by each of three individuals gave a range of weight measurements of 0.001 g, of length measurements of 0.000,5 in., and of diameter measurements of 0.001,1 in. A propagation-of-error analysis indicated that the uncertainty of bulk-density determinations due to limitations of measurement accuracy was less than 0.008 g/cm^3 .

The bulk densities of individual rods are listed in Appendix A, together with their electrical resistivities and Young's moduli. Average density was 1.901 g/cm^3 with extreme values of 1.894 and 1.909 g/cm^3 and standard deviation of 0.002,8 g/cm^3. Comparison of the standard deviation with the calculated uncertainty of measurements suggests that the scatter of measured density values resulted principally from the measuring system used. Bulk density of the graphite was essentially constant throughout the lot, and was unusually high for an unimpregnated graphite.

B. Porosity

Mercury-porosimetry measurements were made on 12 specimens of AAQ1 graphite selected to represent both the most-dense and the least-dense rods in the lot. Data were treated using the finite-interval statistical model, with the results listed in Table VI. Average total porosity, from density measurements, was 15.9% of the specimen volume. Average porosity accessible to mercury at 2600 psi, the highest pressure used, was 3.1% of the specimen volume, or only about 20% of the total porosity. While mercury-porosimetry data must be interpreted with caution, the traditional analysis of data collected on AAQ1 graphite indicates a maximum pore diameter of about 35μ and a median pore diameter of

about 0.4μ.

C. Elastic Properties

1. Young's Modulus

Longitudinal Young's modulus of each rod of AAQ1 graphite was determined individually at room temperature by a thin-rod resonance technique, and is listed in Appendix A. Average dynamic Young's modulus for the entire lot was 2.308×10^6 psi, with extreme values of 2.225×10^6 and 2.364×10^6 psi and standard deviation of 0.0197×10^6 psi. A propagation-of-error analysis indicated that by the method used this modulus could be measured with an uncertainty of about 0.83%, or approximately $\pm 0.02 \times 10^6$ psi. Most measured values fell within this limit, which is very nearly the standard deviation of the measurements. Again, an extremely uniform graphite is indicated.

TABLE VII

TEMPERATURE DEPENDENCE OF LONGITUDINAL YOUNG'S MODULUS OF AAQ1 GRAPHITE, ROD 86

Temperature, C	E, 10^6 psi
25	2.330
200	2.330
300	2.350
400	2.365
500	2.385
600	2.410
700	2.435
800	2.465
900	2.495
1000	2.54
1200	2.65
1400	2.78
1600	2.93
1800	3.04
2000	3.15
2200	3.23
2300	3.28
2350	3.29
2400	3.29
2450	3.27

A series of measurements of dynamic Young's modulus as a function of temperature was made on one longitudinal specimen from Rod 86. A thin-rod resonance technique was used, and a high temperature of 2476°C was reached with an acceptable signal reading. Results are listed in Table VII and plotted in Fig. 11. Dynamic Young's modulus increased with temperature to a maximum value near 2350°C, with no apparent minimum between room temperature and this maximum. The specimen tested showed little change in modulus with repeated heating and cooling, and no hysteresis upon sudden cooling from about 900 to 450°C.

Static Young's modulus was determined during initial loading of previously unstrained longitudinal specimens in the tensile tests described below, both at room temperature and as a function of temperature between ambient and 2750°C. As is discussed in a later section in connection with the tensile testing procedure, these data are not considered to be of high quality --although part of the broad scatter shown in Fig. 11 is believed to be real and characteristic of the first loading of small samples of a porous solid. The dashed line has simply been sketched through the scatter to suggest the probable trend of the data.

At low and moderately elevated temperatures, these results indicate an initial static modulus which is only about one-half to two-thirds of the dynamic modulus. (In a few tests involving load cycling or repeated loading, the static value appeared to increase toward the dynamic one as the specimen was repeatedly strained.) Above about 1500°C the quality of the static measurements improved, data scatter diminished, and initial static modulus decreased--while dynamic modulus continued to increase to about 2300°C. (In a few tests in this temperature region, static modulus appeared not to be changed significantly by limited amounts of prestrain.) These results suggest the possible existence at high temperatures of a "relaxed" modulus which is very much lower than the "unrelaxed" one measured dynamically, and which decreases quite rapidly as temperature increases

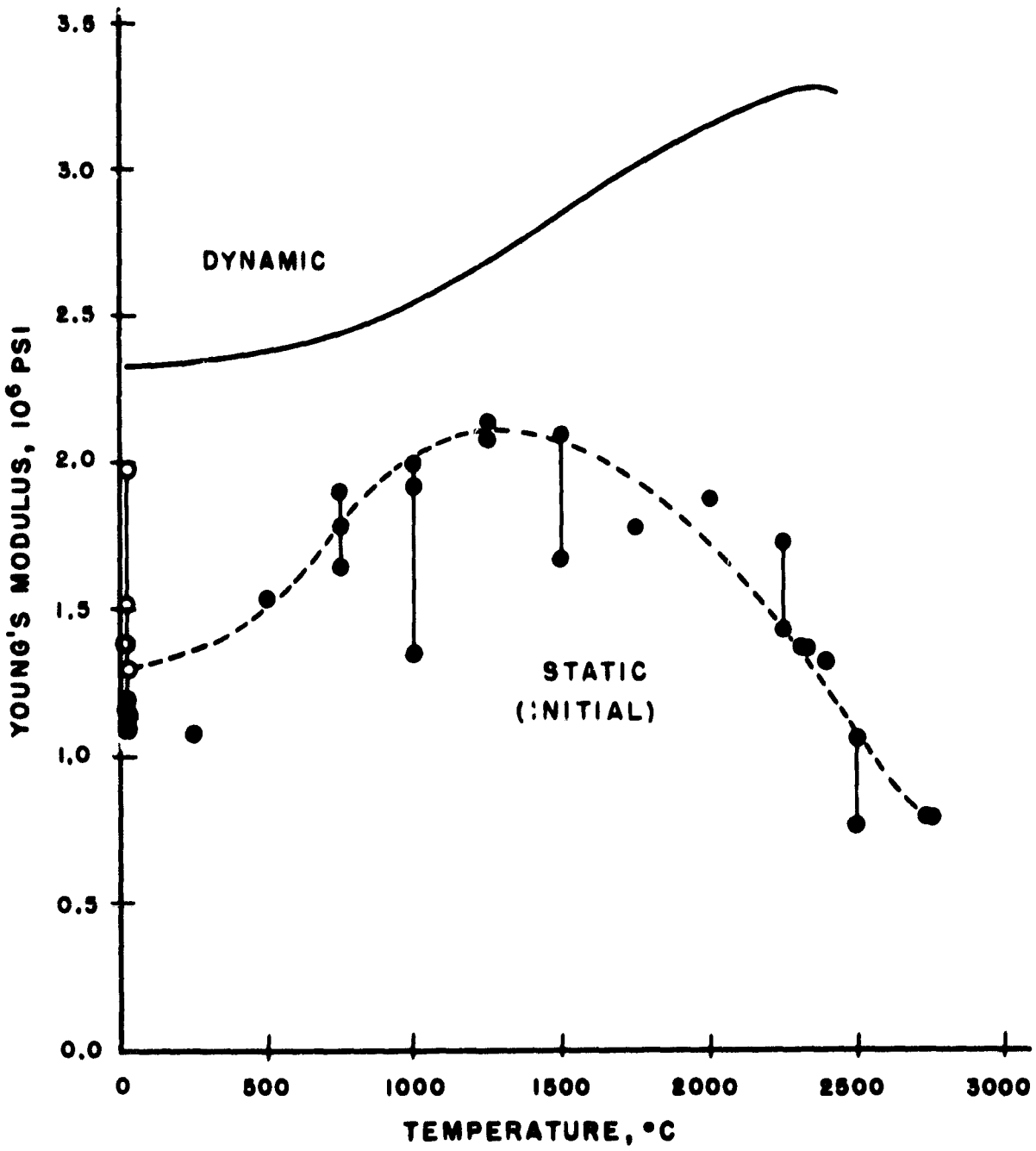

Fig. 11. Longitudinal Young's modulus of AAQ1 graphite.

above about 1500°C.

In an attempt to resolve the differences between static and dynamic values of Young's modulus, both types of measurements were made at room temperature on specimens 0.25-in. dia, 10-in. long, machined from Rods 15, 35 and 39. Static measurements were made in a low-level stress-strain apparatus in which slowly applied dead-weight loading is used to develop tensile stresses up to about 22 psi, and strain is measured with an unbonded strain gage. Dynamic measurements were made by a thin-rod resonance technique. Densities of the three specimens were 1.907, 1.915,and 1.907 g/cm^3, in agreement with the microradiographic observation of a relatively dense region along the extrusion axis. Dynamic Young's moduli were 2.375 x 10^6, 2.386 x 10^6, and 2.375 x 10^6 psi, respectively, correlating well with densities. In spite of precise instrumentation, careful measurements, and use of a very low stress range, static modulus values scattered broadly and erratically from specimen to specimen and during successive cycles of loading and unloading

the same specimen. The most probable static moduli for the three specimens were judged to be 2.12×10^6, 2.01×10^6, and 2.25×10^6 psi, respectively. Load vs extension records were generally curved (convex upward) during the first cycle or two of loading, becoming essentially linear in later cycles. A lower loading rate (4.5 psi/min) usually -- but not always -- gave lower and less consistent modulus values than did a higher rate (9.0 psi/min). Modulus measured during loading was usually -- but not always -- lower than that measured during subsequent unloading. The static moduli determined were significantly less than the dynamic moduli of the same specimens, but were much higher than those measured in regular tensile tests and plotted in Fig. 11. These differences reflect the deficiencies of the strain-measuring system used for the tensile tests, and also suggest either that the stress-strain curve for AAQ1 graphite is strongly curved at unresolvably low stresses or that, even at room temperature, a time-dependent relaxation occurs to reduce the apparent modulus in a "static" test.

A cylinder 0.250,2-in. dia was cored from Rod 93, leaving intact a shell of material 0.081,8-in. thick which included the extrusion skin. Density of the core was 1.907 g/cm^3 and its longitudinal dynamic Young's modulus was 2.35×10^6 psi, in reasonable agreement with the results noted above. Density and dynamic modulus of the shell were 1.889 g/cm^3 and 2.29×10^6 psi, respectively.

Because of the small diameter of the graphite rods, Young's modulus normal to the extrusion axis could not be measured. However, room-temperature measurements were made at 3 MHz of longitudinal pulse-transmission velocities both parallel and normal to the extrusion axis. One sample from Rod 86 was used. In the axial direction pulse velocity was 1.182×10^5 in./sec and in the transverse direction it was 0.872×10^5, giving a velocity ratio of 1.36. This ratio, when squared, indicates that the corresponding bulk-modulus ratio was 1.84 which, to a good approximation, should represent the anisotropy of AAQ1 graphite with regard to Young's modulus.

2. Shear Modulus

Shear modulus normal to the extrusion direction was determined on one specimen by an eddy-current technique involving the use of closely fitting aluminum sleeves on each end of the specimen. The dynamic shear modulus so measured was 0.748×10^6 psi. As discussed below, pulse-velocity measurements also indicated a significant degree of anisotropy with regard to shear modulus.

3. Pulse-Transmission Velocities

In this type of material, the difference between thin-rod and bulk pulse-transmission velocities depends on degree of anisotropy and Poisson's ratio. For an isotropic material, theory predicts a ratio of bulk velocity to thin-rod velocity of unity when Poisson's ratio is zero, of 1.01 when Poisson's ratio is 0.1, of 1.05 when Poisson's ratio is 0.2, and of 1.16 when Poisson's ratio is 0.3. For one AAQ1 graphite specimen, the thin-rod velocity was 1.141×10^5 in./sec (giving $E = 2.33 \times 10^6$ psi in the axial direction) and the bulk velocity in the same direction was 1.182×10^5 in./sec. The small ratio between the two, 1.033, may be evidence that Poisson's ratio of this graphite is very small.

Measurements of shear pulse-transmission velocities at 3 MHz were also made at room temperature on the same sample. Three measurements made with the propagation direction parallel to the extrusion direction but with different polarization directions gave the same pulse velocity, $(6.21 \pm 0.03) \times 10^4$ in./sec, indicating that the extrusion axis was an axis of symmetry with regard to elastic behavior. Measurements of velocity perpendicular to the extrusion axis gave values of 6.47×10^4 in./sec when the polarization direction was parallel to the extrusion axis and of 5.46×10^4 in./sec when it was perpendicular to that axis. The lower of these transverse shear velocities is about 12% less than the average axial shear velocity (6.21×10^4 in./sec), suggesting a significant degree of anisotropy with regard to shear modulus. The average axial velocity should have been identical with the torsional thin-rod value, 6.48×10^4 in./sec. The 4% difference, however, is within the expected combined

uncertainty of the two methods.

D. Tensile Properties

1. Room Temperature Tests

Six groups of longitudinal specimens of AAQ1 graphite have been tested in tension at room temperature, with the results listed in Table VIII. Specimen numbers are the numbers of the rods from which individual test bars were machined, plus a letter A, B, or C indicating, respectively, the end of the rod extruded first, its central region, and its trailing end. The "standard" test bar used had a gage section 1.00-in. long, tapering in diameter by about 0.003 in. from its ends to a minimum 0.250-in. dia at its center. The gage section terminated in 0.047-in. radii leading to 0.344-in.-dia end sections, providing a square shoulder against which tracking markers could be seated for optical strain measurements.

The first group of eight specimens listed in Table VIII was tested in air in a system usually used for elevated-temperature testing, at a constant rate of crosshead motion of 0.005 in./min. Removable tracking targets were attached to both specimen shoulders, and were observed with an Optron optical tracking system. This may have produced a small asymmetry in loading. However, the average ultimate strength determined, 3004 psi, was relatively high for a well-graphitized material, and the standard deviation of the measurements was only 4.6% of the average. Percent permanent elongation, from measurement of reassembled broken test bars, averaged 0.14%, which is normal for a polycrystalline graphite. Stress-strain curves, from optical-tracking data, are plotted in Appendix C. Strain data collected during the early stages of loading were in general of poor quality, principally because of erratic small changes in specimen position as it aligned itself with the tension axis. Static Young's modulus values derived graphically from the stress-strain curves were correspondingly uncertain. However, as would be expected in initial loading of previously unstrained graphite, they indicated a relatively broad variation in initial Young's modulus from specimen to specimen, and an initial static modulus which was only about one-half to two-thirds of the dynamic modulus reported above. All stress-strain curves were slightly convex upwards, and six of them grouped well. The other two, for specimens 20A and 65B, were steeper, suggesting that these specimens might have been prestrained accidentally at some point in their earlier history.

A second group of three specimens was tested under the same conditions but by another operator in a different testing machine, using a different type of loading fixtures and without tracking markers. One relatively low strength value was measured, but the average ultimate strength (2903 psi) was not significantly different from that of the first group.

The third "group" was a single subsize specimen, No. 68C, machined to 0.200-in. gage diameter but otherwise identical with the standard specimens of the first two groups. It was tested in the elevated-temperature unit, without tracking markers, to verify that the use of subsize specimens in some of the high-temperature tests discussed below had no large effect on the strength measurement. Its ultimate strength was slightly above the average for larger-diameter specimens, as might be expected from the density gradient observed in the extruded rod, but was within the scatter of those other measurements. Its permanent elongation was very low but, as seen in Appendix B, this was not characteristic of subsize specimens.

The three specimens composing the fourth group of Table VIII were standard specimens tested in the low-temperature unit, without tracking markers, at a rate of crosshead motion four times that usually used. No significant change in ultimate strength was observed from this relatively small increase in strain rate.

The fifth specimen group consisted of four specimens tested at their full as-extruded cross sections by use of metal grips cemented to the ends of unmachined rod sections. Tests were made in the low-temperature machine without tracking markers at 0.020 in./min crosshead motion. Data scatter was relatively broad, and it is not clear that the full cross-section rod differed in strength from the reduced section tested in the case of machined specimens. If there was a difference, however, it was a small in-

TABLE VIII

LONGITUDINAL TENSILE PROPERTIES OF AAQ1 GRAPHITE TESTED AT ROOM TEMPERATURE

Specimen No.	Specimen Type	Type of Test	Test Atmosphere	Ultimate Tensile Strength psi	Elongation (3 inch),	Initial Young's Modulus 10^6 psi
1A	Standard, 0.250 in. dia	Tension, 0.005 in. min.	Air	2985	0.13	1.[illegible]9
2A	Standard, 0.250 in. dia	Tension, 0.005 in. min.	Air	3093	0.09	1.[illegible]8
2B	Standard, 0.250-in. dia	Tension, 0.005 in. min.	Air	2986	0.14	1.09
6B	Standard, 0.250 in. dia	Tension, 0.005-in. min.	Air	3113	0.21	1.[illegible]1
8A	Standard, 0.250-in. dia	Tension, 0.005-in. min.	Air	2875	0.15	1.38
89A	Standard, 0.250-in. dia	Tension, 0.005 in. min.	Air	3244	0.11	1.17
106A	Standard, 0.250-in. dia	Tension, 0.005-in. min.	Air	2863	0.12	1.19
121A	Standard, 0.250-in. dia	Tension, 0.005-in. min.	Air	2872	0.14	1.38
Average	Standard, 0.250-in. dia	Tension, 0.005-in. min.	Air	3004	0.14	1.37
σ	Standard, 0.250-in. dia	Tension, 0.005-in. min.	Air	137	0.04	0.28
10A	Standard, 0.250 in. dia	Tension, 0.005-in./min.	Air	2975	---	---
10B	Standard, 0.250-in. dia	Tension, 0.005-in./min.	Air	2689	---	---
10C	Standard, 0.250-in. dia	Tension, 0.005-in./min.	Air	3044	---	---
Average	Standard, 0.250-in. dia	Tension, 0.005-in. min.	Air	2903	---	---
σ	Standard, 0.250-in. dia	Tension, 0.005-in./min.	Air	188	---	---
68C	Subsize, 0.200-in. dia	Tension, 0.005-in./min.	Air	3167	0.03	---
17A	Standard, 0.250-in. dia	Tension, 0.020-in./min.	Air	3178	---	---
17B	Standard, 0.250-in. dia	Tension, 0.020-in./min.	Air	3178	---	---
17C	Standard, 0.250-in. dia	Tension, 0.020-in./min.	Air	2893	---	---
Average	Standard, 0.250-in. dia	Tension, 0.020-in./min.	Air	3083	---	---
σ	Standard, 0.250-in. dia	Tension, 0.020-in./min.	Air	164	---	---
113A	Full cross-section rod	Tension, 0.020-in./min.	Air	3083	---	---
113B	Full cross-section rod	Tension, 0.020-in./min.	Air	3632	---	---
64A	Full cross-section rod	Tension, 0.020-in./min.	Air	3368	---	---
64B	Full cross-section rod	Tension, 0.020-in./min.	Air	3068	---	---
Average	Full cross-section rod	Tension, 0.020-in./min.	Air	3288	---	---
σ	Full cross-section rod	Tension, 0.020-in./min.	Air	268	---	---
12B	Standard, 0.250-in. dia	Tension, 0.005-in./min.	He, 3 psig	3015	0.09	1.14
52C	Standard, 0.250-in. dia	Tension, 0.005-in./min.	He, 3 psig	2836	0.10	1.09
82B	Standard, 0.250-in. dia	Tension, 0.005-in./min.	, 3 psig	2997	0.13	1.16
Average	Standard, 0.250-in. dia	Tension, 0.005-in./min.	He, 3 psig	2949	0.10	1.13
σ	Standard, 0.250-in. dia	Tension, 0.005-in./min.	He, 3 psig	99	0.02	0.04

crease in strength from retention of the extra-low skin, which is contrary to what would be expected from the density and modulus gradients described above.

The last group of specimens listed in Table VIII was tested in the high-temperature unit in a static helium atmosphere at 3 psig, which was introduced after the specimen and furnace chamber had been degassed by evacuating to a residual pressure less than 10^{-4} torr. Tracking targets and the optical strain-measuring system were used, and stress-strain curves are plotted in Appendix C. There was no significant difference between these results and those of tests made in air, and agreement with results from adjacent specimens (12A, 12B, 82C) tested in air was extremely good. The stress-strain curves produced grouped well with the less steep curves for tests made in air, and were unexpectedly consistent in initial slope.

Most specimens failed by brittle fracture near one of the radii terminating the straight sections, suggesting some degree of notch-sensitivity or of misalignment of the specimen and tension axes. Fracture surfaces were finely granular in appearance and in general were quite flat and approximately normal to the tension axis. Microscopic examinations of sections through fracture surfaces revealed that fracture paths were partly through binder residue, partly through filler particles, and partly along interfaces between the two. This is discussed in the next section.

Although variations in testing equipment, strain rate, specimen diameter, and ambient atmosphere appear to have increased the ranges of the tensile properties measured, there is no evident reason to exclude any of the values listed in Table VIII from calculation of the room-temperature properties of AAQ1 graphite. Including them all, the average ultimate tensile strength was 3052 psi with a standard deviation of 201 psi; average permanent elongation in 1-in. was 0.13% with a standard deviation of 0.03%; and average initial static Young's modulus was 1.31×10^6 psi with standard deviation of 0.26×10^6 psi.

2. Elevated-Temperature Tests

Tensile tests were made in helium on longitudinal specimens of AAQ1 graphite over the temperature range ambient to 2750°C, with the results plotted in Fig. 12 and tabulated in Appendix B. Specimens were degassed by evacuating the furnace chamber to a residual pressure less than 10^{-4} torr and continuing to evacuate it while the specimen was heated to the desired testing temperature and held for 1 hr. (Residual pressure at temperature was usually less than 2×10^{-4} torr after this outgassing period.) The chamber was then filled with helium to a pressure 3 psi above atmospheric; temperature, pressure, and optical trackers were adjusted over a period of about 10 to 15 min, and the tensile test was made at a constant rate of crosshead motion of 0.005 in./min. However, for tests made at temperatures above 2000 C, final vacuum-degassing was for 1 hr at 2000 C, after which the furnace was filled with helium to 3 psig before the specimen was heated to the testing temperature.

All strength data from these tests have been plotted in Fig. 12, together with notched-bar tests discussed in the next section. Apparently because of a combination of notch-sensitivity, a very rapid increase in strength with temperature, and a high temperature gradient in the specimen ends, most standard specimens tested in the interval 1750 to 2325°C broke prematurely through the threaded specimen ends. Therefore, as is indicated in the figure, several subsize specimens were tested at 2000 to 2400 C.

A 0.2% yield strength distinct from the ultimate strength was first detected at 2250°C. At this and higher temperatures, yield strength has therefore been plotted separately. However, in plotting, yield strength has been offset upward in temperature by 50° to avoid confusion with points representing ultimate strength.

Between room temperature and 1750°C, ultimate tensile strength increased almost linearly with temperature from about 3000 psi at room temperature to about 4250 psi at 1750°. Between 1750 and 2325°C, the strength increase was much more rapid. A relatively sharp strength maximum occurred at about 2325°, at a strength level of about 8050 psi, or approximately 2.7 times the room-temperature value. At higher temperatures, strength decreased rapidly as temperature increased but was still about 4650 psi at 2750°C.

Yield strength at 0.2% offset decreased with increas-

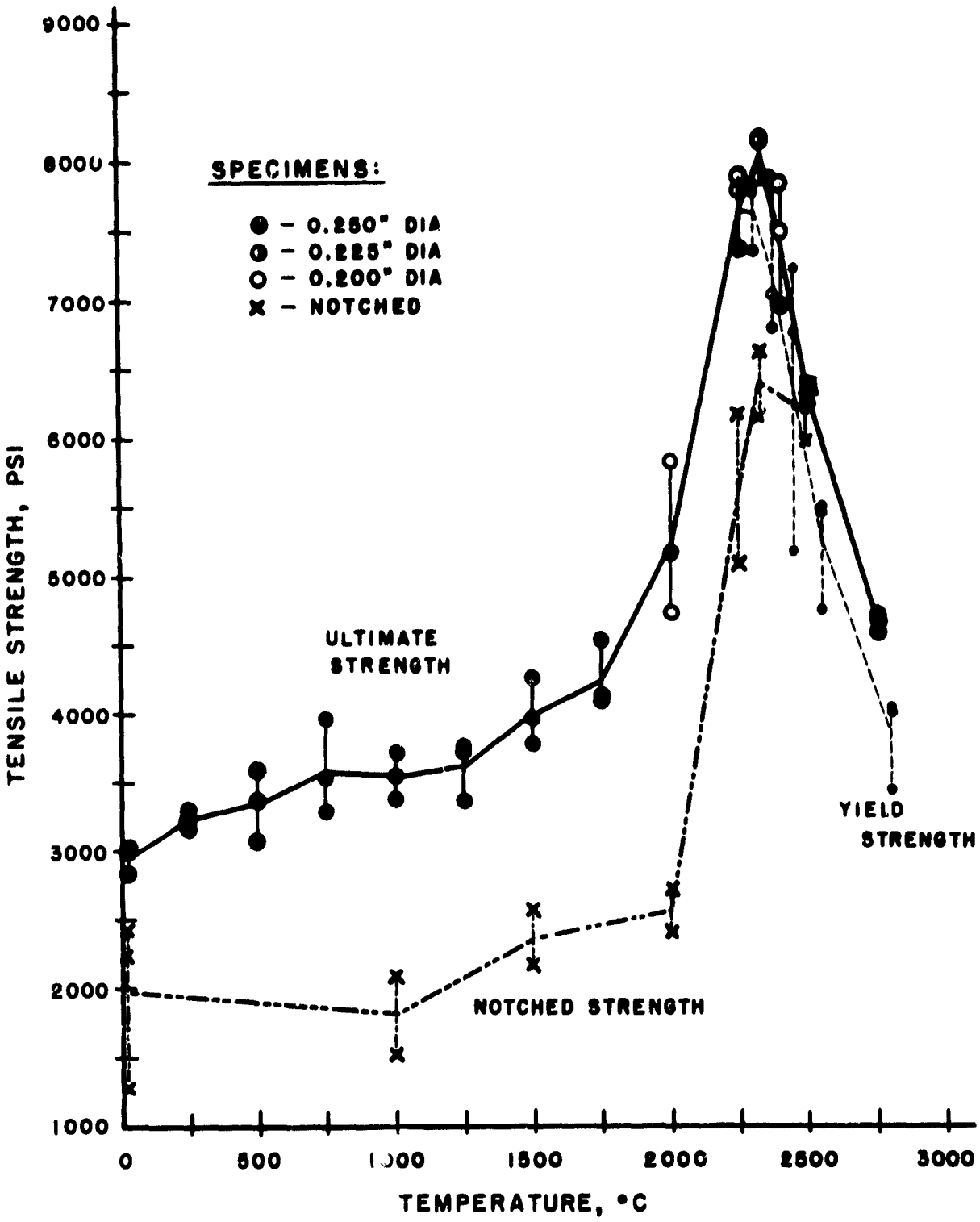

Fig. 12. Longitudinal tensile properties of AAQ1 graphite tested in helium.

ing temperature from the temperature at which it could first be measured, 2250°C, to the highest testing temperature used, 2750°C. The rate at which it decreased was approximately equal to the rate of decrease of ultimate strength with temperature above 2325°C.

As measured at room temperature on reassembled tested specimens, percent elongation of the 1-in.-long gage section was about 0.1% at all temperatures below 2250°C. At higher temperatures it increased slowly with temperature, but was still only about 1.0% at 2750°C,

representing a relatively brittle material. Individual and average values at each testing temperature are tabulated in Appendix B.

Specimen diameter was also remeasured at room temperature on tested specimens. Those tested at 2750° had acquired a surface layer of pyrolytic graphite about 0.001-in. thick, presumably evaporated from the graphite heater tube, which is believed not to have affected their tensile behavior significantly. Those tested at lower temperatures had not changed measurably in diameter, indicating that the small amount of permanent elongation which occurred was produced principally by opening of cracks or other voids in the graphite structure.

Initial static Young's moduli determined in these tests are tabulated in Appendix B; and stress-strain curves plotted from optical tracking data are shown in Appendix C. Because of tracking difficulties,not all tests produced useful stress-strain data and,in several cases indicated by arrows on individual curves, the stress-strain curves used are from other tests in which failure occurred prematurely through the specimen ends or in the loading grips. In general,tracking was better and results more consistent at the higher testing temperatures. The stress-strain curves are in general convex upward, although at 2500 and 2750°C they show an initial region which is nearly linear. Accuracy of the optical strain measurement can be estimated by comparing permanent strain indicated by these curves with percent elongation measured on reassembled specimens, listed in Appendix B. Agreement is not exact but is closer than might have been predicted on the basis of uncertainties in modulus measurements, the anelastic properties of graphite, and the limitations of the tracking system itself. While the data from which these curves were plotted are not of high quality, the curves are believed not to be seriously in error.

At all testing temperatures, fracture surfaces were finely granular in appearance, quite flat and smooth, and approximately normal to the tension axis. However, at temperatures above 2000°C there was some tendency toward less regular, more angular fractures, at angles less than 90° to the stress axis. Fracture location was usually toward the end of the gage section, near or adjacent to the beginning of the radius leading to the specimen shoulder.

The fracture paths were apparently similar in all specimens tested at all temperatures. At low magnification, as illustrated by Fig. 13, the fracture appeared to pass between filler particles almost entirely through binder residue. Higher magnification, however, showed that a significant fraction of the path was either through filler grains or at their interfaces with the binder. Thus, Fig. 14 illustrates cleavage of a filler particle which happened to be oriented so that its lamellar internal structure was approximately parallel to the fracture path. Figure 15 shows a region in which the path was nearly normal to the lamellar structure of a filler grain and, instead of passing through the grain, followed its interface with the binder. However, the usual situation was that illustrated by Fig. 16, in which the fracture was a mixture of intergranular, transgranular, and interfacial with, if anything, a preference for the intergranular path through binder residue. This is contrary to the situation in most high-density pitch-bonded graphites, in which there is a strong preference for transgranular fracture.

Weight loss during testing was normal for a graphite which had previously been heat-treated to a temperature above that at which the test was made. In general it was

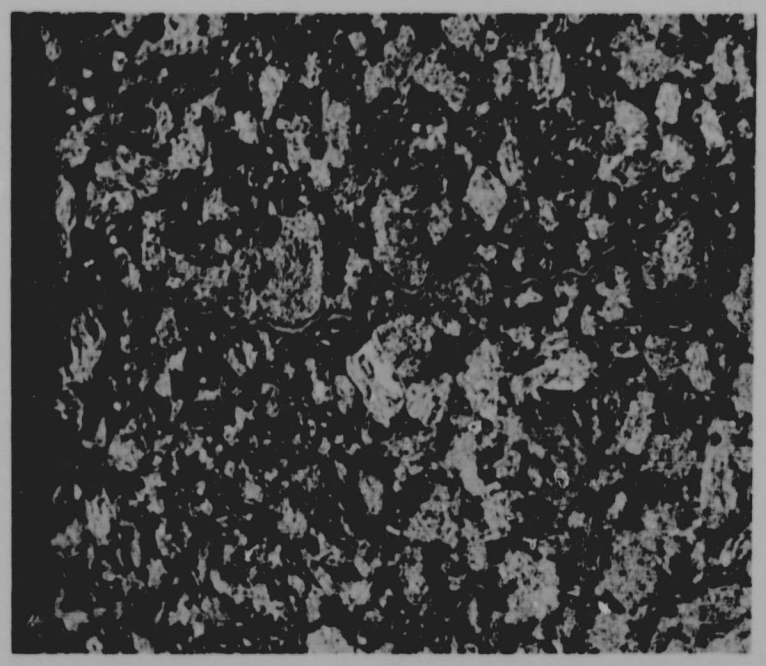

Fig. 13. Fracture path in AAQ1 graphite broken in tension at 2400°C, as revealed by impregnation of reassembled specimen with epoxy mounting resin. Krypton-ion etch; 75 X.

Fig. 14. Cleaved lamellar filler particle. Krypton-ion etch; 7000 X. Reticulated central area is epoxy impregnant separating fracture surfaces. Light areas result from heavy-metal shadowing of replica.

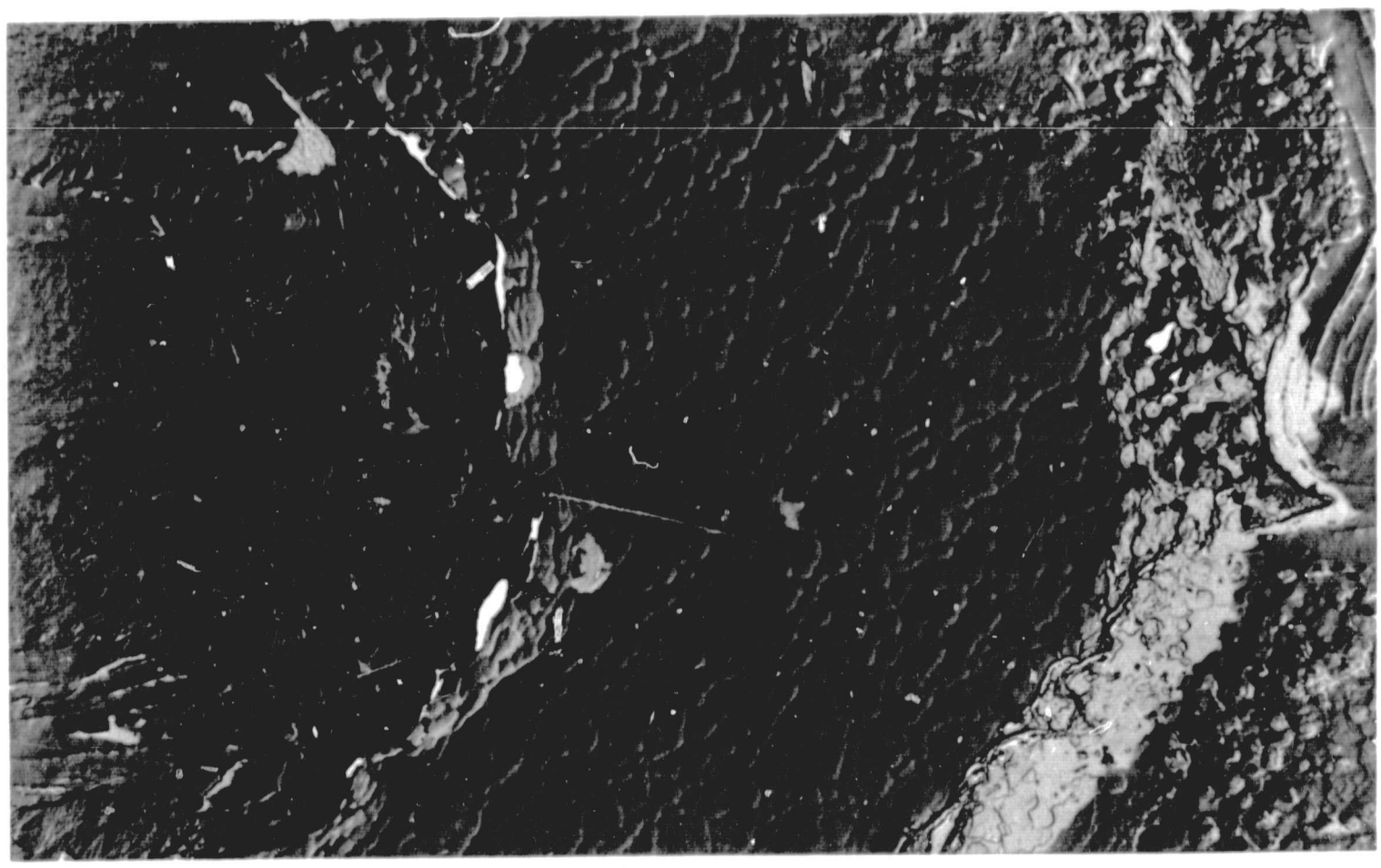

Fig. 15. Fracture along interface between filler particle (left) and binder (right, containing carbon black). Krypton-ion etch; 7000 X.

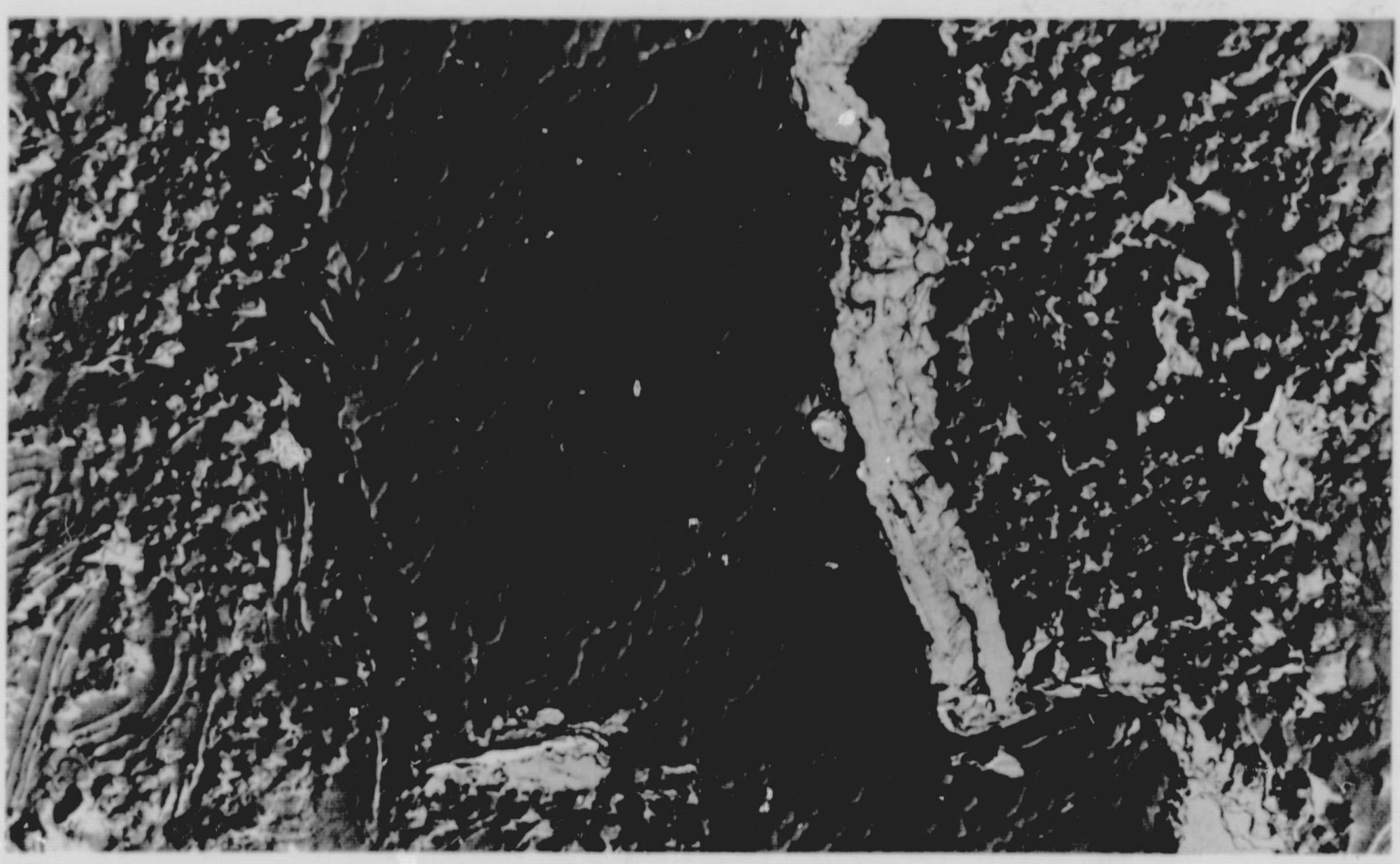

Fig. 16. Mixed fracture, partly through filler, partly through binder residue, and partly at interfaces. Krypton-ion etch; 7000 X.

of the order of hundredths of one percent, and increased only slightly at the higher testing temperatures.

3. Notched-Bar Tests

The fracture behavior described above suggested that AAQ1 graphite was distinctly more sensitive to the presence of notches than were most other graphites which had previously been tested under the same conditions. A qualitative exploration of its notch sensitivity was therefore undertaken by testing a small group of sharply-notched tensile bars at a few different temperatures.

The specimens used were standard 0.250-in.-dia test bars on which the gage diameter had been reduced locally to 0.125 in. by machining a circumferential 60° V-groove at the center of the gage length. Root radius of the groove was 0.001,4 to 0.001,7 in. which, according to Peterson's curves,[2] produces a stress-concentration factor, K_t, of about 4.5. Tests were in helium at a constant rate of crosshead motion of 0.005 in./min, under the same conditions used for unnotched tensile tests. Results are listed in Table IX and plotted in Fig. 12.

Except for one low value at room temperature, the notched strength values were unexpectedly consistent. From room temperature to 2000°C, notched strength was about one-half to two-thirds of unnotched strength, indicating a relatively high degree of notch sensitivity--which, if anything, was higher at 2000°C than at room temperature. Above 2000°C, and especially above 2325°C, the degree of notch sensitivity decreased, and at 2500°C the material was essentially as strong with the notch as without it. This suggests that at least a small amount of real plasticity exists in this graphite at 2500°C, and that it may be developing at and above about 2250°C.

4. Diametral Compression Tests

In an attempt to measure the tensile strength of AAQ1 graphite normal to the extrusion direction, diametral compression tests were made in air at room temperature

TABLE IX

ULTIMATE TENSILE STRENGTH AS A FUNCTION OF TEMPERATURE, SHARPLY-NOTCHED TENSION BARS, AAQ1 GRAPHITE, K_t = 4.5

Specimen No.	Test Temperature, °C	Test Atmosphere	Notched Tensile Strength, psi	Unnotched Tensile Strength, psi	Ratio, Notched to Unnotched Tensile Strength
92B	Room	Air	1255		
48C	Room	Air	2414		
49B	Room	Air	2245		
Average	Room	Air	1971	3052	0.65
78A	1000°	He, 3 psig	2100		
102B	1000°	He, 3 psig	1528		
Average	1000°	He, 3 psig	1814	3548	0.51
48A	1500°	He, 3 psig	2566		
5A	1500°	He, 3 psig	2162		
Average	1500°	He, 3 psig	2364	4003	0.59
114A	2000°	He, 3 psig	2747		
36B	2000°	He, 3 psig	2405		
Average	2000°	He, 3 psig	2576	5236	0.49
48B	2250°	He, 3 psig	5100		
5C	2250°	He, 3 psig	6169		
Average	2250°	He, 3 psig	5635	7665	0.74
9C	2325°	He, 3 psig	6145		
114C	2325°	He, 3 psig	6616		
Average	2325°	He, 3 psig	6381	8046	0.79
68B	2500°	He, 3 psig	5958		
49C	2500°	He, 3 psig	6386		
Average	2500°	He, 3 psig	6172	6317	0.98

on 7 full cross-section rod segments machined from Rod 30. Results are listed in Table X. Although they are quite consistent, these strength values are extremely low compared to the longitudinal tensile strength given above, even for a relatively anisotropic material. Results at Battelle Memorial Institute[3] indicate that this is typical of diametral compression tests on graphite. The strength calculated from such a test is said in general to be considerably lower than that measured in direct tension, by a factor which varies from one graphite to another.

Accordingly, the strength values listed in Table X are believed not to be correct on an absolute basis. However, they are expected to be useful for comparing this graphite with other generally similar graphites.

TABLE X

APPARENT TRANSVERSE TENSILE STRENGTH OF AAQ1 GRAPHITE AT ROOM TEMPERATURE, FROM DIAMETRAL COMPRESSION TESTS

Specimen No.	Ultimate Strength, psi
30A	1545
30B	1572
30C	1319
30D	1598
30E	1494
30F	1452
30G	1359
Average	1477
σ	106

E. Compressive Properties

Compressive tests were made in air at room temperature on eight longitudinal specimens of AAQ1 graphite from four different rods. Results are listed in Table XI.

The compression specimens used were full cross-section segments of the extruded rods, each 1.50 in. long. They were tested at a constant rate of crosshead motion of 0.020 in./min between removable tool-steel platens coated on their bearing surfaces with "Fluoro-Glide", a commercial fluorocarbon dry lubricant.[4] No stress-strain data were collected, but the load vs time record made for each test permitted a reasonably accurate estimate of yield strength at 0.2% compression, as an indication of deformation behavior.

In most cases fracture occurred near the center of specimen length, apparently from a combination of shear and transverse tension, with much local shattering of the graphite at the instant of fracture. Permanent increase in specimen diameter could not be measured accurately because of gross cracking associated with the fracture, but in general appeared to be between 0.1 and 0.3% and to average about 0.2%. Because of extensive shattering, only one specimen could be reassembled for a measurement of reduced length, and even this measurement was very uncertain. It indicated a permanent decrease in specimen length of approximately 2.1% as a result of the compression test.

The ratio of ultimate compressive strength to ultimate tensile strength was 3.58, which is normal for a graphite.

TABLE XI

ROOM-TEMPERATURE COMPRESSIVE PROPERTIES OF AAQ1 GRAPHITE

Specimen No.	Ultimate Compressive Strength, psi	Yield Strength (0.2%), psi
2C	11,430	9,560
2D	11,188	9,896
44C	10,386	9,269
44D	11,133	9,865
90C	10,922	9,438
90D	10,453	9,304
117C	10,977	9,770
117D	10,839	9,642
Average	10,916	9,593
σ	357	243

F. Flexural Strength

Room-temperature flexure tests were made on four full cross-section longitudinal segments of AAQ1 rod, using four-point loading over a 4-in. span. Results are listed in Table XII. The ratio of ultimate tensile strength to

TABLE XII

ROOM-TEMPERATURE FLEXURAL STRENGTH OF AAQ1 GRAPHITE

Specimen No.	Ultimate Strength, psi
56A	4676
56B	5022
63A	4802
63B	4959
Average	4865
σ	156

flexural strength was 0.63, which is of the magnitude reported for most other graphites.

G. Creep Properties

Short-time tensile creep tests were made on longitudinal specimens of AAQ1 graphite at 2300 and 2500°C in a static helium atmosphere. The specimens used had gage length of 1.00 in. and gage diameter of 0.220 in. They were outgassed by heating in vacuum to about 2100°C, after which the furnace chamber was filled with helium to a pressure 2 psi above atmospheric, which was maintained during further heating and testing. Creep loads were applied through a lever system by hanging weights. Strains were measured on a magnified image of the specimen, projected onto a screen, by use of a pair of travelling microscopes equipped with micrometer eyepieces. A change of 0.000,5 in. in specimen length could be resolved readily, permitting strain increments of 0.05% to be measured with confidence. The creep strains reported are measured total strains minus elastic strains calculated from the applied unit load and the dynamic Young's modulus at the testing temperature.

To evaluate the uniformity of this graphite and the reproducibility of the testing procedure, 15 tests were made at 2500°C and 5260 psi tensile stress. The creep curves produced are plotted in Fig. 17. Under these conditions, creep rates became essentially constant after the specimens had been under load for about 5 min. These "constant" creep rates are listed in Table XIII, together with time to rupture and strain to rupture. For this group of tests, standard deviation of the apparent steady-state creep rate was about 18% of the average. The estimated uncertainty in creep rate due to possible stress variations (of not more than 1.25%) was ± 10%. That due to temperature variations (of not more than 10°C) was ± 20%. The consistency of the creep results indicates that testing conditions were also consistent, and that the properties of the graphite--and presumably its structure--were very uniform from specimen to specimen.

Creep rates from tests at 2300 and 2500°C are shown as functions of tensile stress in Fig. 18, where they are compared with Seldin's results[5] for with-grain specimens of commercial ATJ graphite. In all cases creep rates were much lower for AAQ1 than for ATJ graphite at the

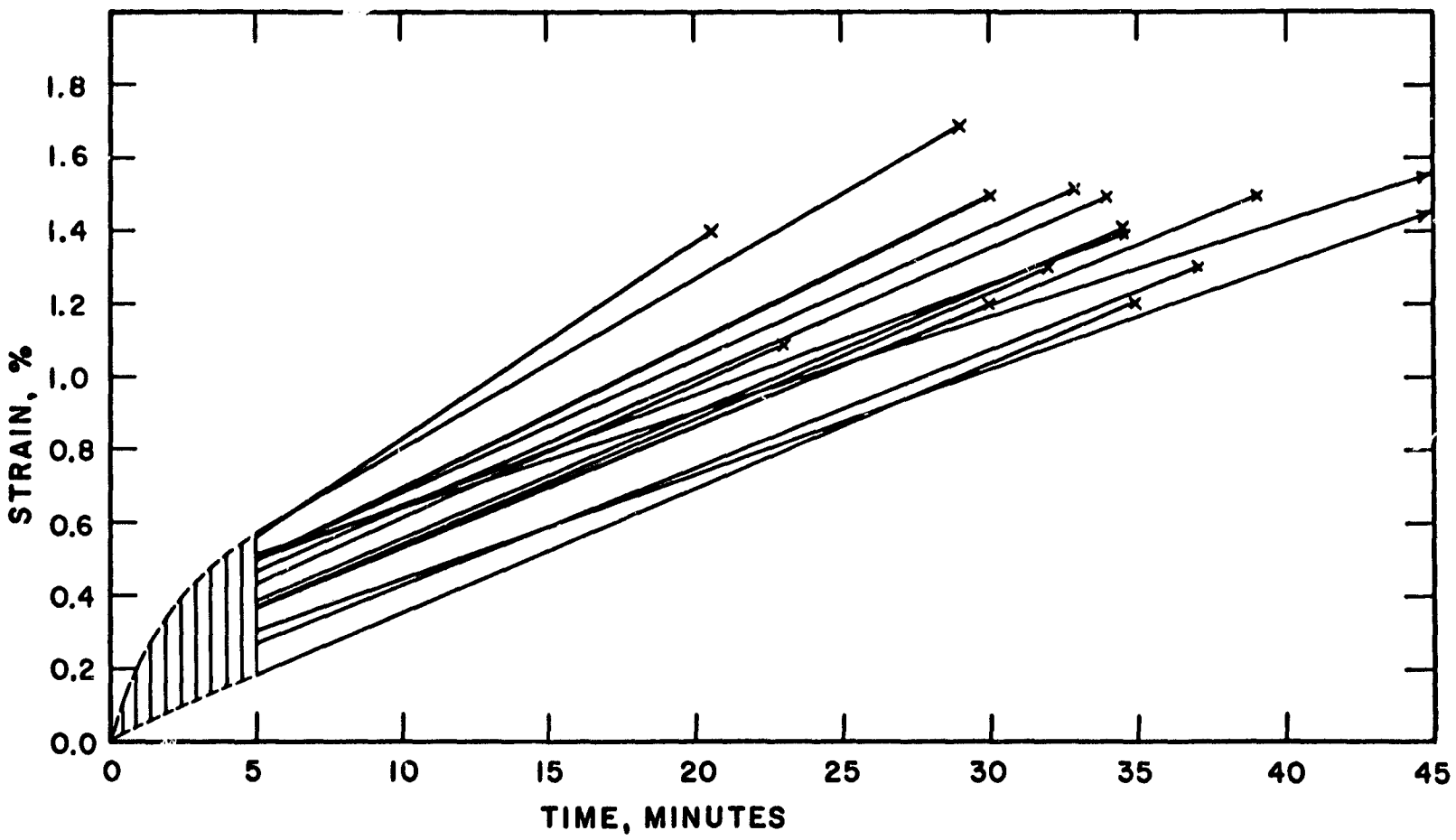

Fig. 17. Creep curves for AAQ1 graphite tested at 2500°C and 5260 psi tensile stress, "X" indicates fracture.

TABLE XIII

TENSILE CREEP PROPERTIES OF AAQ1 GRAPHITE AT 2500°C AND 5260 PSI

Specimen No.	Creep Rate, (in./in.) x 10^{-4}/min.	Strain to Rupture, %	Time to Rupture, Min.
45A	3.3	1.3	37
45B	2.6	1.7	50
45C	3.3	1.2	30
23A	5.1	1.4	21
23B	3.4	1.2	35
23C	3.4	1.5	34
110A	3.4	1.3	32
110B	3.5	1.4	34
110C	3.7	1.1	23
30A	4.7	1.7	29
30B	3.3	1.5	39
30C	2.9	1.6	50
95A	4.0	1.5	30
95B	3.8	1.5	33
95C	3.2	1.4	34
Average	3.57	1.41	34.0
σ	0.63	0.18	7.8

same temperature and stress. The slopes of the line segments plotted in Fig. 18 indicate that for AAQ1 graphite the apparent steady-state creep rate is proportional to about the eighth or ninth power of stress, whereas for ATJ graphite it is proportional to about the fourth power of stress. The strong stress-dependence of creep rate in the case of AAQ1 graphite was verified by a change-in-stress test at 2500°C, in which creep rates of the same specimen just before and just after a sudden load change were compared. Again creep rate was found to vary as about the eighth power of stress.

Time to rupture is plotted as a function of stress in Fig. 19 for tensile creep tests on AAQ1 graphite at 2300 and 2500°C. The trends of both curves are those which would be expected if, at each temperature, strain to fracture were constant, and indicate that a very large increase in time to rupture is produced by a relatively small decrease in stress.

The apparent activation energy for tensile creep of AAQ1 graphite was determined by three different methods. In the first of these, creep rates of the same specimen at the same stress were compared just before and just after a sudden change in temperature, and the calculated energy requirement was about 250 kcal/mole. In the second method, two supposedly identical specimens were tested at the same stress but at two different temperatures, and their creep rates were compared at the same value of strain. This gave an apparent activation energy of 225 kcal/mole. The third method is like the second in that two specimens were tested at the same stress and different temperatures, but in this case the times required to produce a given amount of strain were compared. This gave an energy of 220 kcal/mole. Agreement among results of the three methods is considered good. However, because it uses only one specimen and thus minimizes the possibility of differences in specimen structure when the measurements are made, the first of these methods is believed to be the

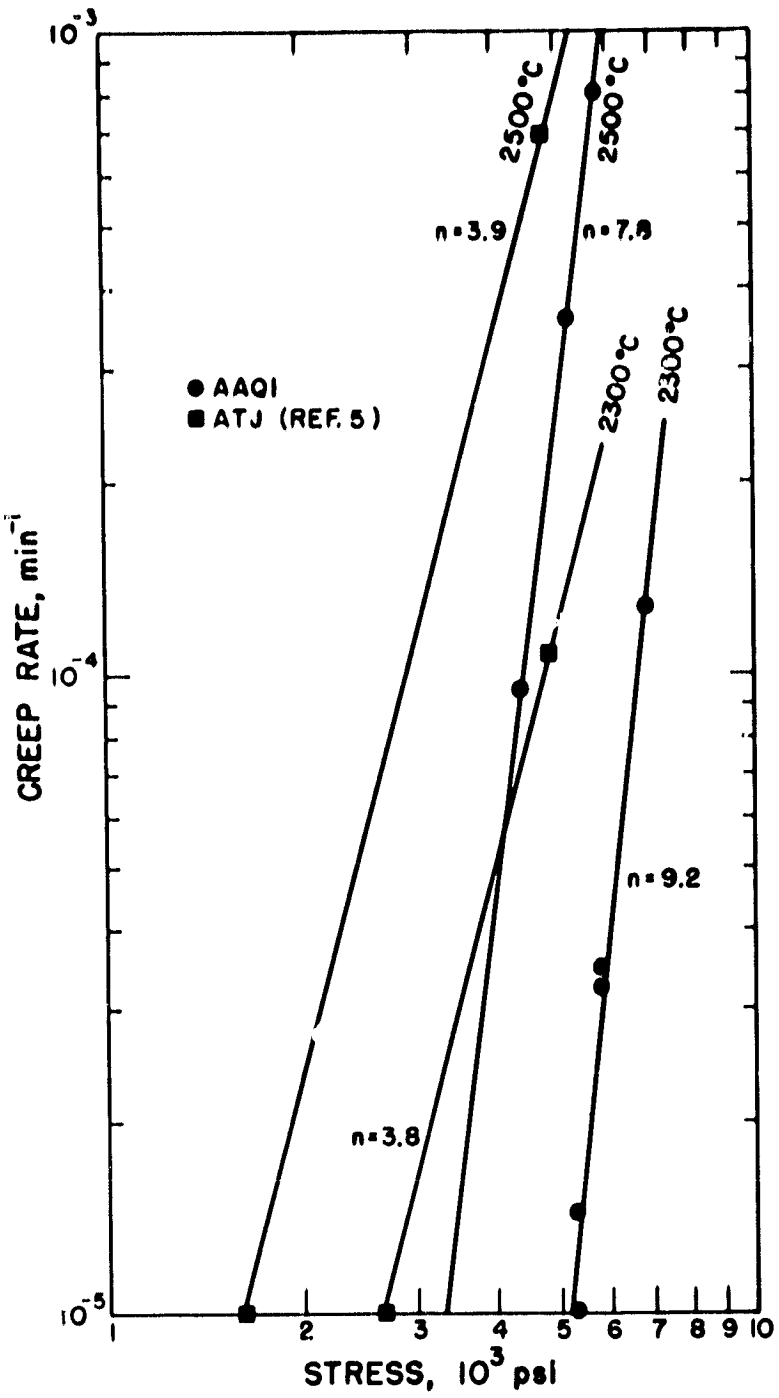

Fig. 18. Tensile creep rate vs stress for AAQ1 and ATJ graphites at 2300 and 2500°C.

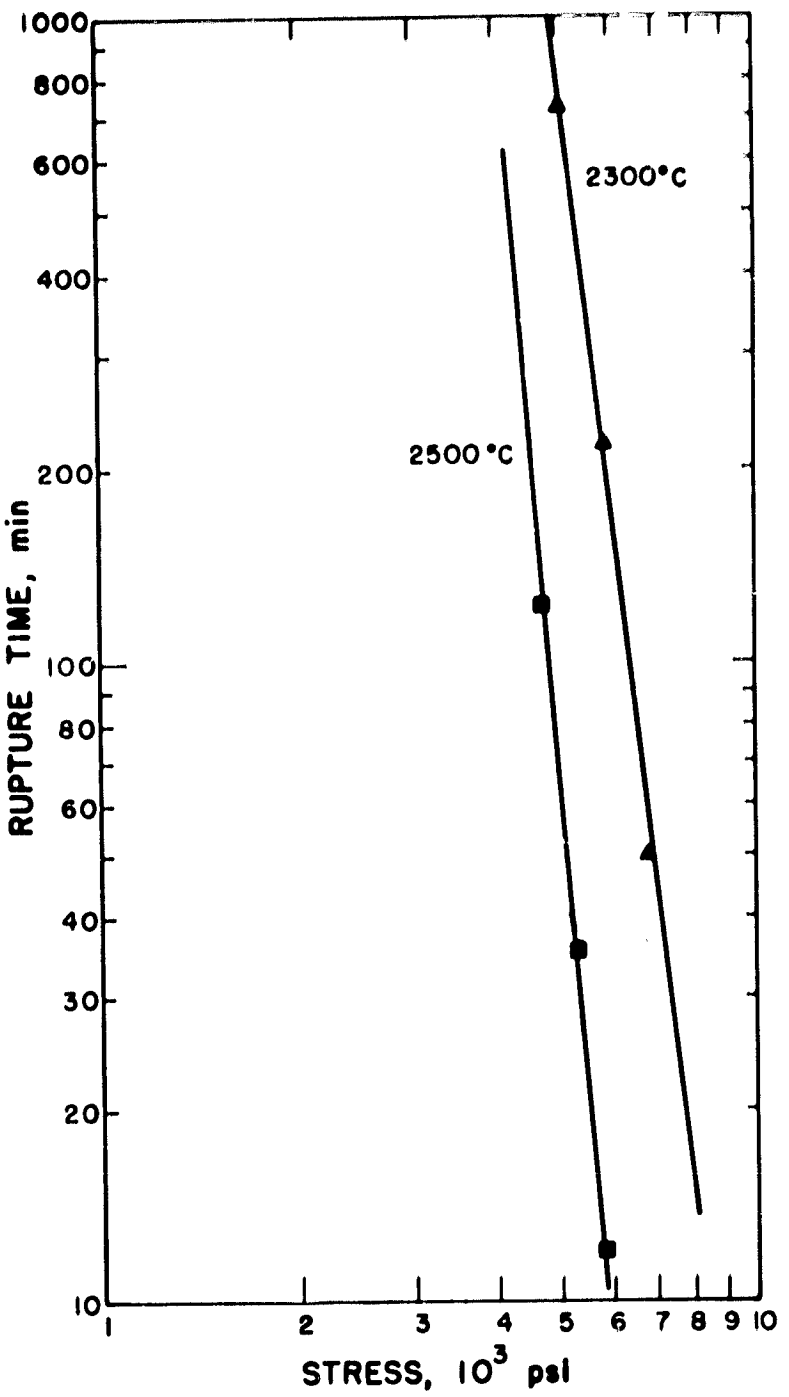

Fig. 19. Time to rupture vs tensile stress for AAQ1 graphite at 2300 and 2500°C.

most reliable, and the value 250 kcal/mole is preferred.

H. Thermal Expansion

The thermal expansion of AAQ1 graphite parallel to the extrusion direction has been measured by three investigators using five different dilatometers. One investigator used a quartz dilatometer over the range 20°K (liquid hydrogen) to 300°K on one specimen machined from Rod 93. The second used another quartz dilatometer over the range 76°K (liquid nitrogen) to 350°K on this same specimen, and an optical dilatometer over the range 25 to 2475°C on a longer specimen from Rod 86. The third investigator used a different quartz dilatometer over the range 25 to 700°C on three specimens--the one from Rod 93 used by the others, and one specime each from Rods 28 and 80. He also used a second optical dilatometer over the range 950 to 2500°C on specimens from Rods 34 and 75. All optical measurements were made on relatively long (~9 cm) specimens to minimize refractive effects.

All data collected by the three investigators were plotted together, and the single "parallel" curve shown in Fig. 20 was drawn so that every experimental point was

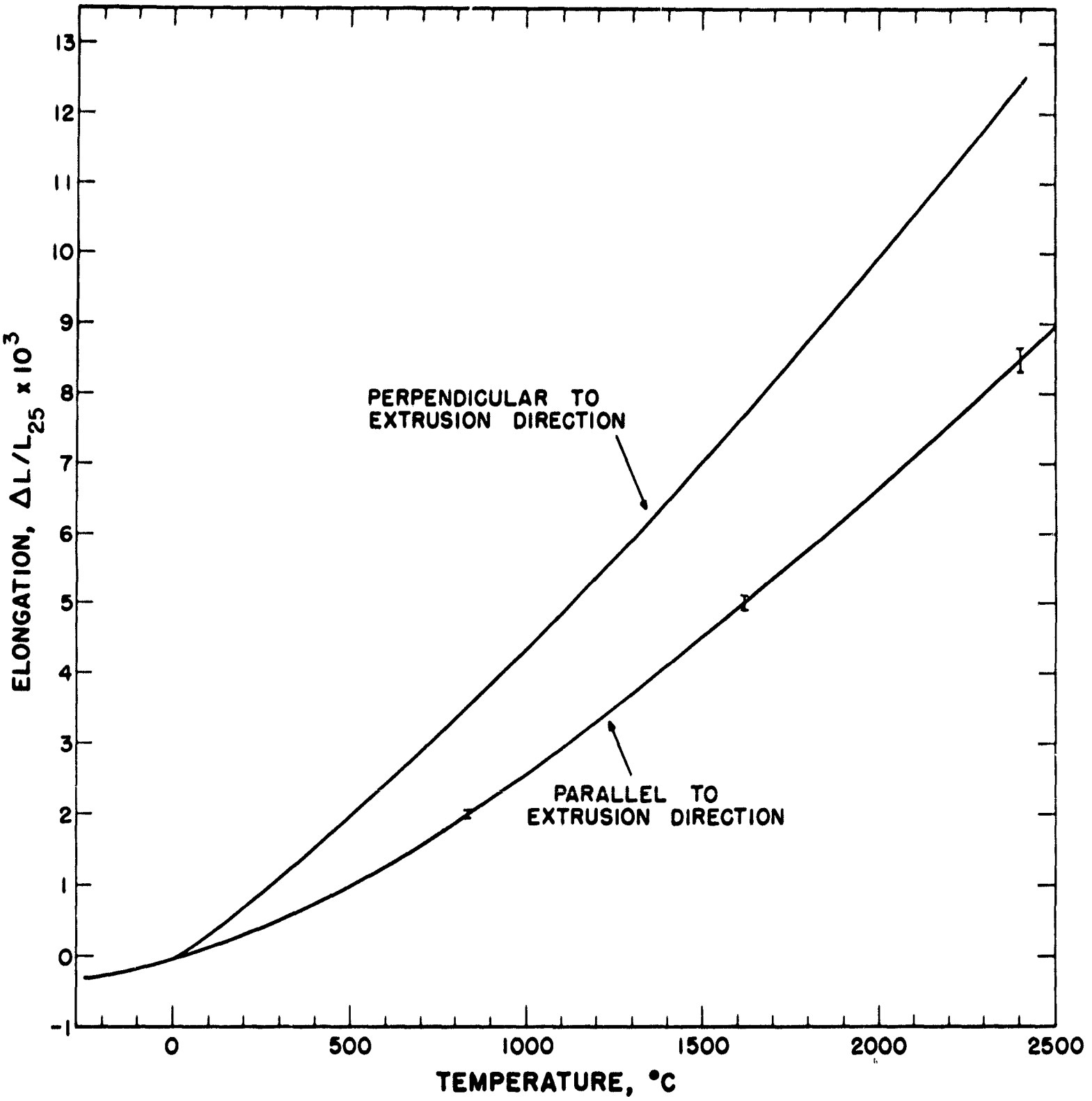

Fig. 20. Thermal expansion of AAQ1 graphite.

contained in a band whose upper and lower envelopes were 4% above the curve and below the curve, respectively. The vertical bars in the figure represent estimated standard deviations.

Thermal expansion perpendicular to the extrusion direction was measured only by the third investigator, using a quartz dilatometer over the range 25 to 700°C and an optical dilatometer over the range 950 to 2450°C. Specimens were built up from stacked discs, each of which was machined so that its cylinder axis was normal to the extrusion direction. Two specimens were used over each temperature interval, one built up of discs from Rod 28 and the other of discs from Rod 80. All data are well represented by the upper curve of Fig. 20.

As would be expected from the expansion properties of the graphite single crystal and from the type of preferred orientation known to exist in this manufactured graphite, the coefficient of linear thermal expansion of AAQ1 graphite is greater normal to the extrusion axis than parallel to it. Near room temperature its anisotropy in this regard is large, the ratio of the two mean expansion coefficients being about 3. However, as is illustrated by Fig. 21, the ratio of the mean values between 25 C and any higher temperature decreases rapidly as the temperature span widens. When the upper temperature is 500°C the ratio is about 2, and when it is 2000°C the ratio is about 1.5. At still higher temperatures it continues to decrease at a diminishing rate.

Qualitatively, this effect of temperature on the anisotropy of thermal expansion can be explained in terms of the effects of a temperature change on in-plane and out-of-plane thermal vibrations of carbon atoms bonded covalently within planes and by van der Waals' forces between planes. However, the rate of change of anisotropy ratio with temperature is higher than might have been expected from the moderate degree of crystalline anisotropy revealed by x-ray diffraction.

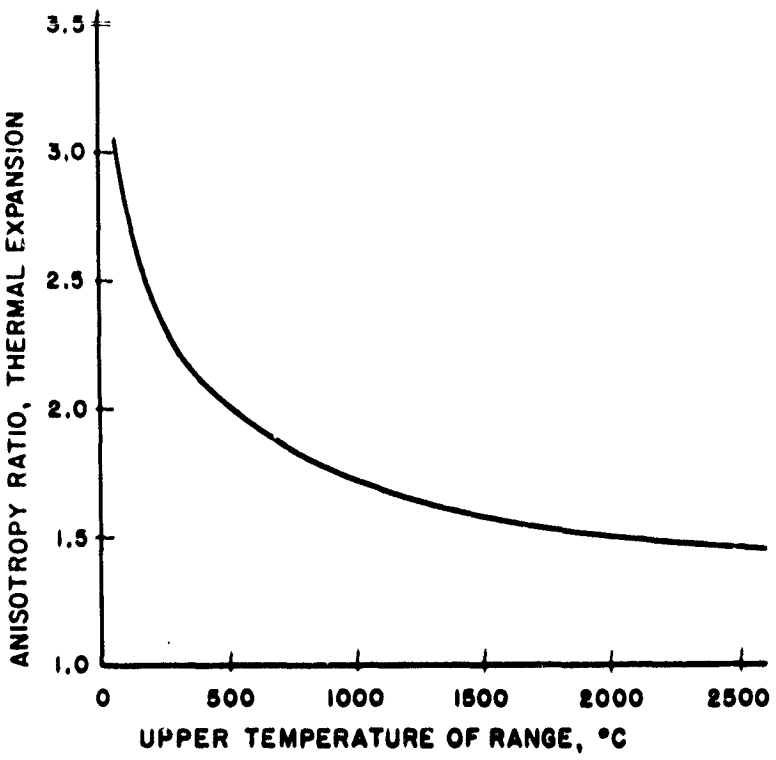

Fig. 21. Thermal-expansion anisotropy of AAQ1 graphite as a function of temperature. The ordinate is the ratio of mean thermal expansion coefficients, perpendicular and parallel to the extrusion direction, between 25°C and the temperature given on the abscissa.

1. Thermal Conductivity

Over the temperature interval -150 to 500 C, the thermal conductivity of AAQ1 graphite normal to the extrusion axis was measured by the flash-diffusivity technique,[6,7] Between 840 and 2500 C, it was measured by a radial heat-flow method[6,7] involving a resistively-heated rod radiating to a cold environment, and measurement of the temperature difference between the bottoms of two adjacent cylindrical holes drilled radially into the rod to different depths. In the latter method, specimen temperature was measured with a disappearing filament optical pyrometer and temperature difference between holes by a differential radiation pyrometer developed especially for this purpose. However, when specimen temperature was above 2000 C this difference became large enough so that it could also be measured with the optical pyrometer with good accuracy.

All data collected on thermal conductivity measured normal to the extrusion axis are plotted in Fig. 22.

Thermal conductivity parallel to the extrusion axis was measured over the temperature interval -140 to 325 C by the flash-diffusivity method. From 210 to 575 C, it was measured by a series-comparison method using Armco Iron comparison standards. From 600 to about 750°C, the same method was used but with molybdenum as the comparison standard. Above 1000 C, the method used was that of Jain and Krishnan[8] for determining thermal conductivity along the axis of a resistively-heated rod radiating freely in an evacuated environment.

All data collected on thermal conductivity measured parallel to the extrusion axis are plotted in Fig. 23.

Room-temperature thermal conductivities parallel and normal to the extrusion axis, computed from thermal-diffusivity measurements, were 1.26 W/cm-°C and 0.75 W/cm-°C, respectively, yielding an anisotropy ratio of 1.68. This ratio remained essentially constant to at least 1000°C and probably applies reasonably well throughout the entire temperature range covered experimentally. Comparison of the curves of Fig. 22 and 23 suggests that the degree of anisotropy may decrease slightly above 1000°C. However, experimental difficulties inherent in the linear heat-flow method make longitudinal

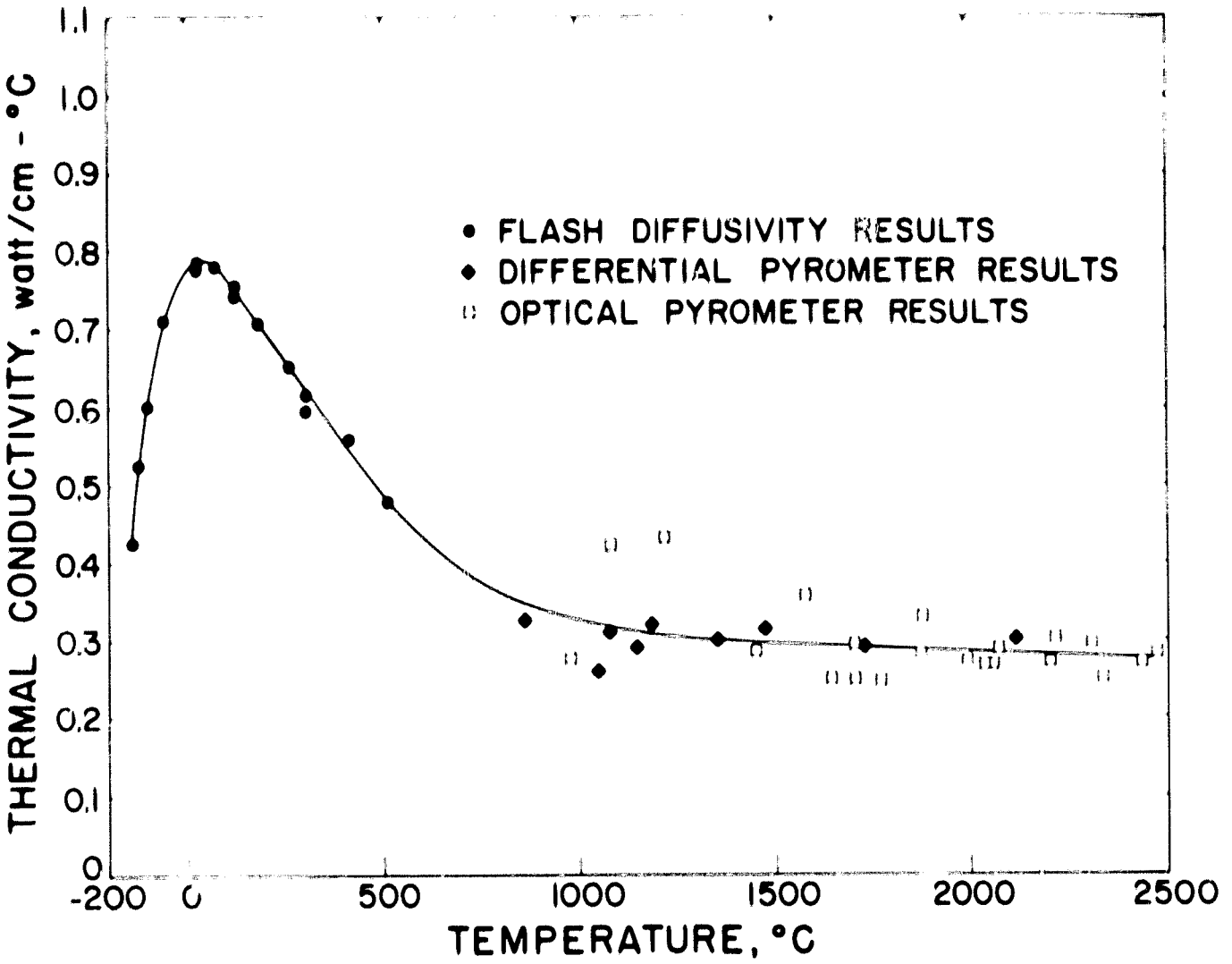

Fig. 22. Thermal conductivity of AAQ1 graphite measured normal to the extrusion direction.

conductivity measurements in this temperature region relatively uncertain, and it is not clear that the apparent decrease is real.

J. Emissivity

Total hemispherical emissivity of the unmachined surface of the graphitized extruded rod was 0.69 over the temperature range 1000 to 1500°C. This is low for a graphite but not unreasonably so in view of published values for polished graphite surfaces and the lustrous appearance of the AAQ1 graphite rods.

K. Electrical Resistivity

Electrical resistivity of each rod of Lot AAQ1 graphite was measured parallel to the extrusion direction by use of a Kelvin double bridge, and is listed in Appendix A. Average resistivity of all rods was 1160 μΩcm, with extreme values of 1090 and 1183 μΩcm and standard deviation of 12.4 μΩcm. Uncertainty of the measurement is believed to be about ± 1%, which is very close to the standard deviation of the measurements. Again, an unusual degree of uniformity is indicated throughout the lot.

Electrical resistivity parallel to the extrusion axis was also measured as a function of temperature over the range ambient to 2300°C, with the results plotted in Fig. 24. Since the specimen was heated resistively and radiated freely to a cold environment, radial temperature gradients were known to exist in it. The resistivity measured at each temperature was therefore actually an average over a small temperature interval. However, a calculation of probable error from this source indicates that it was distinctly less than that arising from measurement uncertainties.

Specimens 0.125-in. dia were cored from a group of randomly chosen AAQ1 graphite rods with the cylinder

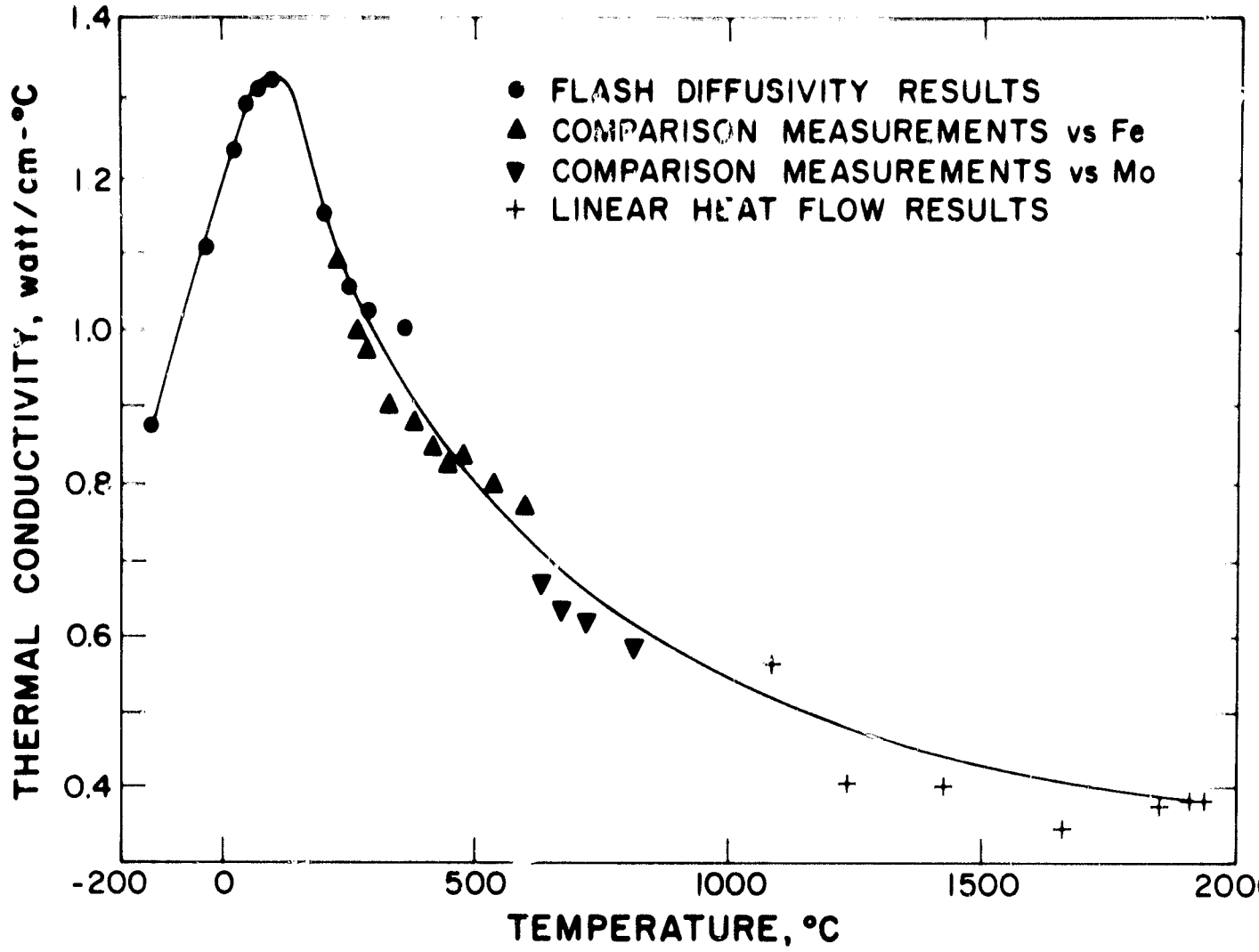

Fig. 23. Thermal conductivity of AAQ1 graphite measured parallel to the extrusion direction.

axes of the specimens either parallel or normal to the extrusion axes of the rods. Average resistivities of these specimens at room temperature were 1133 μΩcm parallel to the extrusion direction and 1901 μΩcm normal to it. Average anisotropy ratio was 1.68, with standard deviation of 0.04. This agrees exactly with the anisotropy ratio computed from room-temperature measurements of thermal conductivity.

VII. CONCLUSIONS

The principal objectives of this experimental program have been accomplished and useful new knowledge has been acquired in several areas which could not have been predicted when the program was undertaken. In particular:

1. A good, large sample of an unusual but useful type of graphite has been produced. It was made from carefully characterized commercial raw materials. Standard manufacturing equipment and techniques were used and detailed records of procedures and conditions were made at every step of the process. If the same raw materials can again be obtained, this graphite can be reproduced.
2. The graphite produced was of high quality and its properties and behavior have been investigated in considerable depth. This represents the first detailed and reasonably complete characterization of a graphite of this type.
3. AAQ1 graphite is one of the most uniform lots of graphite ever produced. In part its uniformity resulted from the care taken in raw-materials preparation and throughout the manufacturing process, particularly in maintaining essentially constant extrusion pressure. Principally, however, it is believed to have resulted from the earlier discovery that much

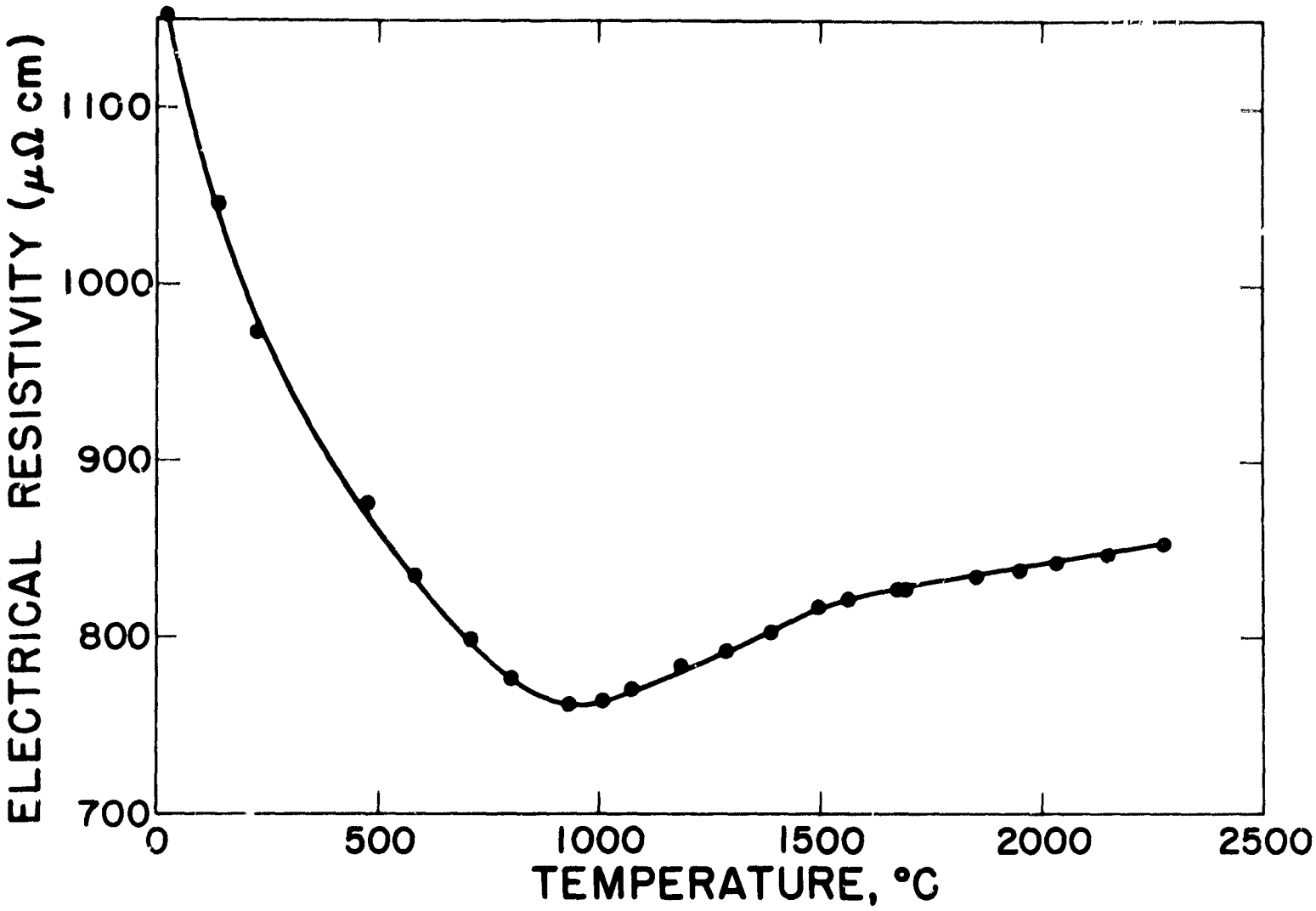

Fig. 24. Electrical resistivity of AAQ1 graphite measured parallel to the extrusion direction.

of the scatter in properties of previous Group CMF-13 graphites was caused by inadequate mixing of raw materials, and from the use in preparing Lot AAQ1 of rather elaborate mixing procedures developed to eliminate this deficiency.

4. The bulk density of AAQ1 graphite, 1.901 g/cm^3, is unusually high for an unimpregnated graphite. This is the joint result of the natures of the raw materials used to make it, of effective mixing of these materials, and of the use of the extrusion process to produce a small-diameter rod. A further small increase in density could probably be achieved by maintaining higher extrusion pressures. Otherwise, it is unlikely that the density of this type of graphite can be increased significantly except by changing the size or shape distributions of the filler materials (graphite flour and carbon black), modifying the molecular distribution and other properties of the binder resin, or supplementing the regular manufacturing procedures with impregnation treatments or hot working.

5. Most manufactured graphites change significantly and unpredictably in dimensions and in elastic properties when they are cycled between room temperature and any moderately elevated temperature (e.g., 1000 or 2000°C). AAQ1 graphite appeared to be completely stable in this respect. The reason for this difference in behavior from other graphites is not known. However, since the changes ordinarily observed are believed to result from spontaneous relief of macroscopic internal stresses residual from manufacturing operations, it suggests either that AAQ1 graphite is essentially free of such stresses or that it does not yield to them in the manner usual for pitch-bonded graphites.

6. AAQ1 graphite is relatively strong at room temperature and its strength increases with temperature

to an unusual degree. The curve representing its ultimate tensile strength as a function of temperature is exceptionally steep between 1750 and 2325°C, peaks quite sharply at the latter temperature, then falls rapidly at higher temperatures. The strength maximum occurs at a temperature perhaps 100° lower than that reported for most other graphites, and the maximum strength is unusually high--above 8000 psi, or about 2.7 times the room-temperatures strength.

7. The curve of dynamic Young's modulus of AAQ1 graphite vs temperature rises to a maximum at a temperature near that of the maximum ultimate tensile strength, a coincidence which is unusual. Although the modulus curve is nearly flat in the region just above room temperature, it shows no minimum here as do the corresponding curves for most other graphites. Measurements of static Young's modulus were unsatisfying, but suggest that during initial loading of previously unstrained material the static modulus is significantly lower than the dynamic modulus over the range ambient to 1500°C. Above 1500°, the static modulus appears to decrease as temperature increases, whereas the dynamic modulus continues to increase with temperature to about 2300°C.

8. Graphites in general are reputed to be relatively insensitive to the presence of notches. However, notched-bar tensile tests show that AAQ1 graphite is quite sensitive at low and moderate temperatures to sharp notches perpendicular to the tension axis. Its sensitivity to notches is greater at 2000°C than at room temperature, but diminishes at temperatures above 2000°C and is essentially gone at 2500°C.

9. Percent elongation in advance of fracture was about 0.1% at all temperatures below 2250°C, which is normal for a manufactured polycrystalline graphite. At higher temperatures it increased slightly with temperature, but remained relatively low both in tensile creep (< 2% elongation at 2500°C) and in low strain-rate tensile tests (~1% elongation at 2750°C). AAQ1 graphite, then, is a relatively brittle material at all temperatures investigated.

10. In moderate-to high-density pitch-bonded graphites, the fracture path is preferentially (although not exclusively) through filler particles. In AAQ1 graphite there is a reasonable incidence both of filler-particle cleavage and of separation along the interfaces between filler particles and binder residue, but there appears to be a weak preference for the fracture path to remain in the binder residue.

11. The degree of preferred orientation in AAQ1 graphite is moderate for a material extruded as small-diameter rod from a mix containing acicular filler particles. Its crystalline anisotropy is described by an M value of 1.64 and a Bacon anisotropy factor of 1.36. For most of its properties, anisotropy ratios are about 1.7. Anisotropy of thermal expansion, however, is much greater than this near room temperature, and diminishes to values distinctly less than 1.7 above about 1000°C.

12. It has commonly been assumed that a thermosetting binder, such as the resin used to manufacture AAQ1 graphite, will carbonize during baking to form a "hard carbon" that will not subsequently graphitize. Previously experiments in Group CMF-13 have shown that, at least for furfuryl alcohol resins in association with normal fillers, this is not generally true, although the crystallite sizes produced may be smaller than those developed by some pitch binders at the same heat-treating temperatures. The Varcum binder in AAQ1 did graphitize at a normal graphitizing temperature, and there is some evidence that the Thermax carbon black may also have graphitized to a significant degree.

13. It is usually misleading to compare directly the properties of different types and grades of graphite because of the property variations introduced by such factors as differences in forming method, section size, graphitizing temperature, and degree of preferred orientation. Thus, the creep properties of AAQ1 graphite have been compared above with those of ATJ graphite, a high-quality commercial grade produced by Carbon Products Division of Union Carbide Corporation, to which other graphites are often compared. ATJ, however, is a molded rather than

an extruded grade, is produced in large blocks rather than small-diameter rod, and is distinctly less anisotropic than is AAQ1. A comparison of creep properties in the across-grain direction, had it been possible, would have been much less favorable to AAQ1, as would a number of other possible property comparisons. Another widely known and well-characterized graphite to which AAQ1 might more appropriately be compared is Great Lakes Carbon Corporation's Grade HLM-85. This is a high-density, fine-grained, extruded, pitch-bonded material, graphitized above 2500°C. In the form of 1- to 3-in.-dia rods, some of its properties are:[9]

Density = 1.83 g/cm^3 (vs 1.90 g/cm^3 for AAQ1)

Anisotropy of thermal conductivity = 1.08 (vs 1.68 for AAQ1)

Anisotropy of electrical resistivity = 1.38 (vs 1.68 for AAQ1)

Dynamic Young's modulus, with-grain = 2.2 x 10^6 psi (vs 2.3 x 10^6 psi for AAQ1)

Tensile strength, with-grain = 2400 psi at room temperature, increasing to about 4000 psi at 2400°C (vs 3000 psi and 8000 psi for AAQ1)

Compressive strength, with-grain = 8300 psi (vs 10,900 psi for AAQ1)

Flexural strength, with-grain = 4100 psi (vs 4900 psi for AAQ1)

Thermal conductivity = 1.63 W/cm-°C with-grain, 1.51 W/cm-°C across-grain (vs 1.26 and 0.75 W/cm-°C, respectively, for AAQ1)

Electrical resistivity = 800 μΩcm with-grain, 1100 μΩcm across-grain (vs 1130 and 1900 μΩcm, respectively, for AAQ1).

Although this comparison is not entirely fair to either graphite, it indicates at least that the mechanical and physical properties of AAQ1 graphite are generally comparable with those of a high-quality, pitch-bonded grade. Consideration of this and other pitch-bonded graphites suggests that AAQ1, and presumably other resin-bonded graphites, have some advantages with regard to direct attainment of high densities, strength properties, and behavior at elevated temperatures, with accompanying disadvantages in thermal and electrical conductivities. However, the larger differences are in fabrication characteristics and cost.

VIII. ACKNOWLEDGMENTS

This work was done under the auspices of the United States Atomic Energy Commission (Contr. W-7405-ENG. 36) through its Space Nuclear Propulsion Office, and with the support of the National Aeronautics and Space Administration (P. O. W-12, 595).

The author has participated in organization of the program described herein and in some of its mechanical-properties investigations. Principally, however, he has served as a compiler and reporter of and commentator on the work of others. The program described has been a joint effort of the entire graphite research section of LASL Group CMF-13, including all of the following staff members and technicians:

P. E. Armstrong	E. M. Wewerka
J. M. Dickinson	E. G. Zukas
D. T. Eash	T. D. Baker
W. V. Green	T. S. Brooks
R. J. Impresciа	L. B. Dauelsberg
L. S. Levinson	K. E. Green
H. D. Lewis	H. J. Martinez
J. A. O'Rourke	T. G. Sanchez
R. D. Reiswig	J. W. Shore
P. Wagner	J. H. Wilson

The chemical analyses reported were performed by LASL Group CMB-1 and the microradiographs were taken by LASL Group GMX-1.

REFERENCES

1. Taub, J. M., and Bard, R. J., "Coated Particle Fuel Elements for UHTREX", Los Alamos Scientific Laboratory Report LA-3378, July, 1965.

2. Peterson, R. E., Stress Concentration Design Factors, New York, John Wiley & Sons, Inc., 1953.

3. Chard, W. C., Battelle Memorial Institute, Columbus, Ohio, Personal Communication.

4. "Fluoro-Glide" is an aerosol suspension of a fluorocarbon dry-film lubricant, manufactured by Chemplast, Inc., East Newark, N. J.

5. Seldin, E. J., Research and Development on Advanced Graphite Materials, Vol. XVIII, High Temperature Tensile Creep of Graphite, National Carbon Co. Report WADD TR 61-72, March, 1964.

6. Wagner, P., and Dauelsberg, L. B., Carbon 5, 271 (1967).

7. Wagner, P., and Dauelsberg, L. B., Carbon (in press, 1968).

8. Jain, S. C., and Krishnan, K. S., Proc. Roy. Soc. A222, 167 (1954); A225, 1 (1954); A225, 7 (1954); A225, 19 (1954); A227, 141 (1955); A229, 439 (1955).

9. Glasser, J., and Glasser, W. J., Directory of Graphite Availability, Second Edition, Air Force Materials Laboratory Technical Report AFML-TR-67-113, August, 1967.

APPENDIX A

CHARACTERIZATION OF INDIVIDUAL RODS COMPOSING LOT AAQ1

Extrusion No.	Rod No.	Density, g/cm^3	Electrical Resistivity Longitudinal, $\mu\Omega$-cm	Young's Modulus, Longitudinal, 10^6 psi
1	1	---	---	---
1	2	1.901	1144	2.295
1	3	1.897	1127	2.288
1	4	1.900	1090	2.306
1	5	1.899	1154	2.312
1	6	1.899	1153	2.296
1	7	1.901	1162	2.309
1	8	1.899	1163	2.297
1	9	1.899	1180	2.292
1	10	1.900	1154	2.294
2	11	1.903	1153	2.321
2	12	1.904	1181	2.326
2	13	1.901	1152	2.323
2	14	1.901	1163	2.319
2	15	1.899	1162	2.311
2	16	1.903	1169	2.319
2	17	1.897	1162	2.302
2	18	1.903	1152	2.302
3	19	1.902	1140	2.328
3	20	1.902	1153	2.327
3	21	1.902	1163	2.364
3	22	1.903	1149	2.312
3	23	1.901	1154	2.311
3	24	1.900	1162	2.299
3	25	1.901	1163	2.299
3	26	1.901	1173	2.303
4	27	1.902	1180	2.319
4	28	1.900	1165	2.300
4	29	1.902	1154	2.305
4	30	1.900	1163	2.294
4	31	1.899	1177	2.301
4	32	1.897	1176	2.302
4	33	1.900	1182	2.295
5	34	1.905	1158	2.333
5	35	1.903	1183	2.308
5	36	1.898	1174	2.294
5	37	1.900	1171	2.324

CHARACTERIZATION OF INDIVIDUAL RODS COMPOSING LOT AAQ1 (Continued)

Extrusion No.	Rod No.	Density, g/cm^3	Electrical Resistivity Longitudinal, μΩ/cm	Young's Modulus, Longitudinal, 10^6 psi
5	38	1.900	1158	2.316
5	39	1.900	1171	2.308
5	40	1.901	1165	2.302
5	41	1.899	1148	2.303
5	42	1.901	1154	2.320
6	43	1.900	1139	2.300
6	44	1.900	1158	2.297
6	45	1.901	1169	2.307
6	46	1.900	1160	2.293
6	47	1.899	1164	2.289
6	48	1.899	1153	2.304
6	49	1.898	1151	2.306
6	50	1.897	1168	2.293
7	51	1.904	1140	2.331
7	52	1.903	1153	2.321
7	53	1.900	1160	2.310
7	54	1.903	1145	2.310
7	55	1.901	1151	2.319
7	56	1.903	1149	2.310
7	57	1.902	1155	2.312
7	58	1.899	1155	2.305
7	59	1.897	1168	2.299
8	60	1.903	1151	2.313
8	61	1.903	1171	2.320
8	62	1.900	1167	2.301
8	63	1.901	1151	2.318
8	64	1.901	1155	2.313
8	65	1.901	1160	2.317
8	66	1.901	1163	2.320
8	67	1.900	1169	2.302
8	68	1.900	1163	2.316
9	69	1.905	1154	2.337
9	70	1.904	1158	2.328
9	71	1.902	1183	2.324
9	72	1.904	1151	2.328
9	73	1.903	1160	2.305
9	74	1.900	1154	2.308

CHARACTERIZATION OF INDIVIDUAL RODS COMPOSING LOT AAQ1 (Continued)

Extrusion No.	Rod No.	Density, g/cm^3	Electrical Resistivity Longitudinal, Ω-cm	Young's Modulus, Longitudinal, 10^6 psi
9	75	1.902	1111	2.323
9	76	1.897	1168	2.310
9	77	1.894	1189	2.288
10	78	1.900	1160	2.306
10	79	1.903	1177	2.300
10	80	1.903	1177	2.294
10	81	1.903	1151	2.309
10	82	1.902	1160	2.293
10	83	1.902	1169	2.299
10	84	1.901	1156	2.291
10	85	1.902	1155	2.313
10	86	1.902	1162	2.307
11	87	1.906	1154	2.311
11	88	1.905	1144	2.323
11	89	1.903	1153	2.318
11	90	1.904	1176	2.323
11	91	1.901	1180	2.294
11	92	1.898	1162	2.299
11	93	1.901	1162	2.307
11	94	1.904	1158	2.307
12	95	1.905	1158	2.327
12	96	1.904	1158	2.317
12	97	1.905	1154	2.312
12	98	1.900	1163	2.303
12	99	1.896	1167	---
12	100	1.899	1163	2.287
12	101	1.898	1163	2.293
12	102	1.896	1163	2.283
12	103	1.896	1158	2.275
13	104	1.902	1158	2.317
13	105	1.901	1163	2.282
13	106	1.900	1153	2.298
13	107	1.899	1151	2.313
13	108	1.896	1178	2.258
13	109	1.895	1162	2.225
13	110	1.894	1173	2.227
13	111	1.900	1167	2.259
13	112	1.895	1177	2.260

CHARACTERIZATION OF INDIVIDUAL RODS COMPOSING LOT AAQ1 (Continued)

Extrusion No.	Rod No.	Density, g/cm^3	Electrical Resistivity Longitudinal, $\mu\Omega$-cm	Young's Modulus, Longitudinal, 10^6 psi
14	113	1.903	1149	2.292
14	114	1.897	1148	2.276
14	115	1.898	1160	2.275
14	116	1.898	1152	2.286
14	117	1.899	1152	2.300
14	118	1.899	1154	2.303
14	119	1.901	1147	2.298
14	120	1.903	1169	2.287
14	121	1.899	1176	2.291
15	122	1.901	1167	2.285
15	123	1.897	1172	2.268
15	124	1.898	1154	2.324
15	125	1.902	1159	2.315
15	126	1.901	1167	2.325
15	127	1.901	1166	2.324
15	128	1.899	1158	2.319
15	129	1.905	1158	2.325
16	130	1.909	1158	---
16	131	1.904	1161	2.305
16	132	1.904	1171	2.319
16	133	1.909	1152	2.356
16	134	1.904	1154	2.345
16	135	1.905	1151	2.346
16	136	1.903	1147	2.339
16	137	1.899	1158	2.322
16	138	1.898	1167	2.310
17	139	1.907	1147	2.333
17	140	1.904	1154	2.320
17	141	1.906	1154	2.325
17	142	1.902	1152	2.322
17	143	1.903	1167	2.320
17	144	1.903	1164	2.328
17	145	1.904	1154	2.326
17	146	1.897	1172	2.317
17	147	1.903	1167	2.316
Average	All	1.901	1160	2.308
Maximum	All	1.909	1183	2.364
Minimum	All	1.894	1090	2.225
σ	All	0.0028	12.4	0.0197

APPENDIX B

TENSILE PROPERTIES OF AAQ1 GRAPHITE TESTED IN STATIC HELIUM (3 PSIG) AT 0.305/ MIN

Specimen No.	Test Temperature, C	Ultimate Tensile Strength, psi	Yield Strength, 0.2 % Offset, psi	Elongation (1 inch), %	Initial Young's Modulus, 10^6 psi
12B	Room	3015	---	0.09	1.14
52C	Room	2836	---	0.10	1.09
82B	Room	2997	---	0.13	1.16
Average	Room	2949	---	0.10	1.13
σ	Room	99	---	0.02	0.04
27C	250	3156	---	0.05	1.07
96B	250	3302	---	0.10	---
57C	250	3238	---	0.06	---
Average	250	3232	---	0.07	1.07
σ	250	73	---	0.03	---
85C	500	3359	---	0.06	---
111B	500	3070	---	0.05	---
61C	500	3597	---	0.07	1.54
Average	500	3342	---	0.06	1.54
σ	500	264	---	0.01	---
65C	750	3291	---	0.08	1.90
106C	750	3510	---	0.10	1.78
88A	750	3952	---	0.12	1.65
Average	750	3584	---	0.10	1.78
σ	750	337	---	0.02	0.13
13A	1000	3709	---	0.07	1.35
66B	1000	3546	---	0.09	2.00
27B	1000	3388	---	0.06	1.92
Average	1000	3548	---	0.07	1.76
σ	1000	161	---	0.02	0.35
42B	1250	3362	---	0.10	---
61A	1250	3725	---	0.09	2.08
57A	1250	3755	---	0.06	2.14
Average	1250	3614	---	0.08	2.11
σ	1250	219	---	0.02	0.04

TENSILE PROPERTIES OF AAQ1 GRAPHITE TESTED IN STATIC HELIUM (3 PSIG) AT 3,000 MIN (Continued)

Specimen No.	Test Temperature, °F	Ultimate Tensile Strength, psi	Yield Strength, 0.2 % Offset, psi	Elongation (1 inch), %	Initial Young's Modulus, 10^6 psi
20B	1500	3788	---	0.10	2.10
27A	1500	4269	---	0.06	---
72B	1500	3952	---	0.09	1.67
Average	1500	4003	---	0.08	1.89
σ	1500	245	---	0.02	0.30
20C	1750	4108	---	0.13	1.78
66A	1750	4080	---	0.11	--
61B	1750	4536	---	0.05	---
Average	1750	4241	---	0.10	1.78
σ	1750	256	---	0.04	---
111C	2000	5167	---	0.12	---
92C[a]	2000	5833	---	0.17	---
41A[a]	2000	4709	---	0.07	---
Average	2000	5236	---	0.12	1.88[b]
σ	2000	565	---	0.05	0.22[b]
82C	2250	7347	7347	0.29	1.73
2B[c]	2250	7775	7775	0.40	1.44
36C[a]	2250	7874	7786	0.14	---
Average	2250	7665	7636	0.28	1.59
σ	2250	280	146	0.13	0.21
44A[c]	2325	8130	7856	0.54	1.37
117B[c]	2325	7864	6771	0.38	1.57
79A[a]	2325	8144	7044	0.28	---
Average	2325	8046	7224	0.40	1.47
σ	2325	158	510	0.13	0.14
41C[a]	2400	7824	6742	0.45	---
79C[a]	2400	7481	7223	0.33	---
121C	2400	6940	5166	0.50	1.32
Average	2400	7415	6377	0.43	1.32
σ	2400	446	1076	0.09	---

TENSILE PROPERTIES OF AAQ1 GRAPHITE TESTED IN STATIC HELIUM (3 PSIG) AT 0.00[illegible] MIS (Continued)

Specimen No.	Test Temperature, C	Ultimate Tensile Strength, psi	Yield Strength, 0.2 % Offset, psi	Elongation (1 inch),	Initial Young's Modulus, 10^6 psi
16B	2500	6369	5500	0.71	0.77
17B	2500	6356	5468	0.69	
8A	2500	6225	4744	0.87	1.01
Average	2500	6317	5237	0.72	0.89
σ	2500	80	428	0.11	0.21
16C	2750	4715	3443	0.98	
8B	2750	4588	4048	0.92	0.83
9A	2750	4657	4003	1.10	0.93
Average	2750	4653	3831	1.00	0.83
σ	2750	64	337	0.09	0.06

a. 0.200-in. dia

b. For three specimens whose stress-strain curves are plotted in Appendix C

c. 0.225-in. dia

APPENDIX C

STRESS-STRAIN CURVES FOR LONGITUDINAL SPECIMENS OF AAQ1 GRAPHITE TESTED AT 0.005 IN./IN.-MIN.

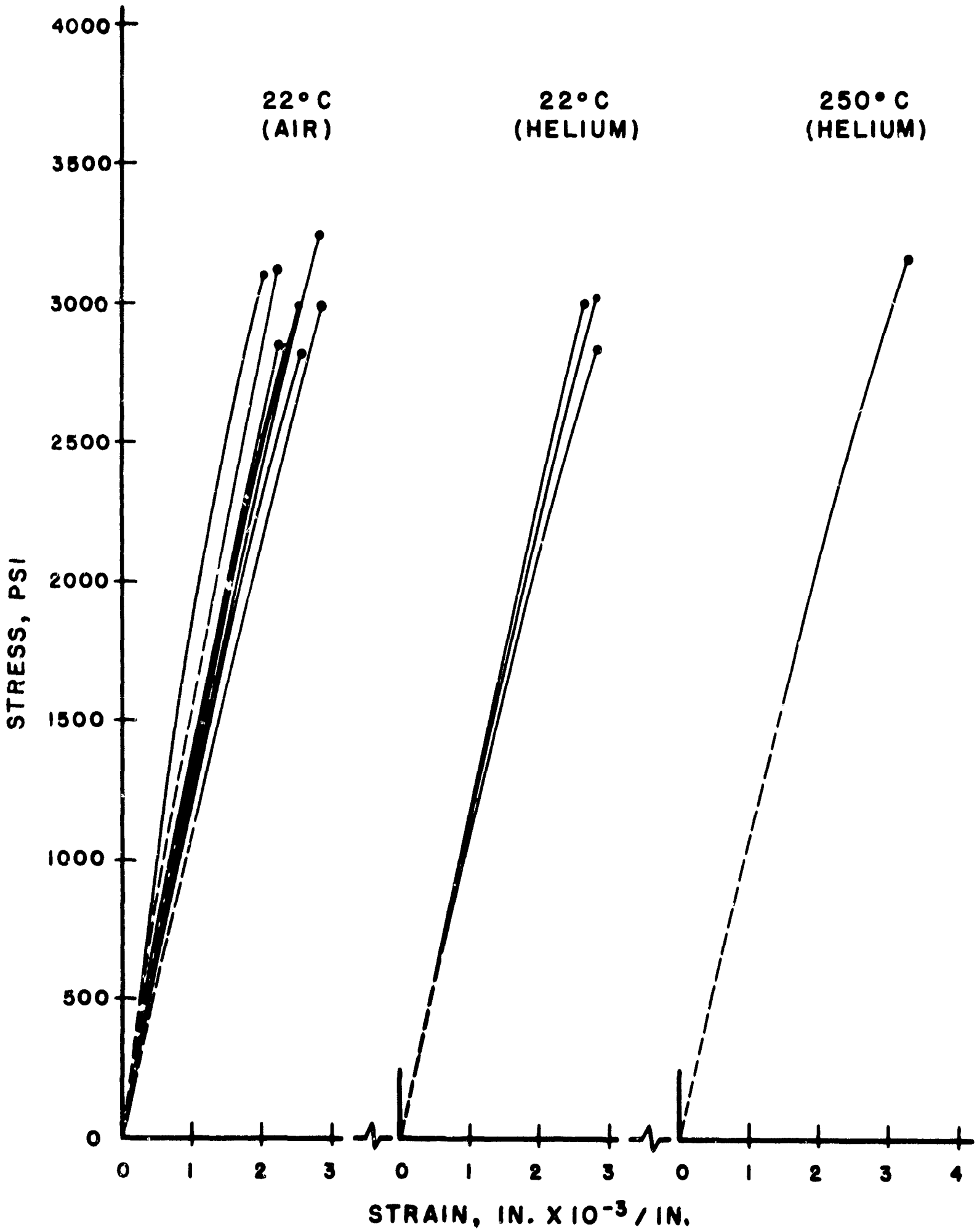
22° C
(AIR)
22° C
(HELIUM)
250° C
(HELIUM)
STRESS, PSI
4000
3500
3000
2500
2000
1500
1000
500
0
0
1
2
3
0
1
2
3
0
1
2
3
4
STRAIN, IN. X 10⁻³ / IN.

Figure C-1.

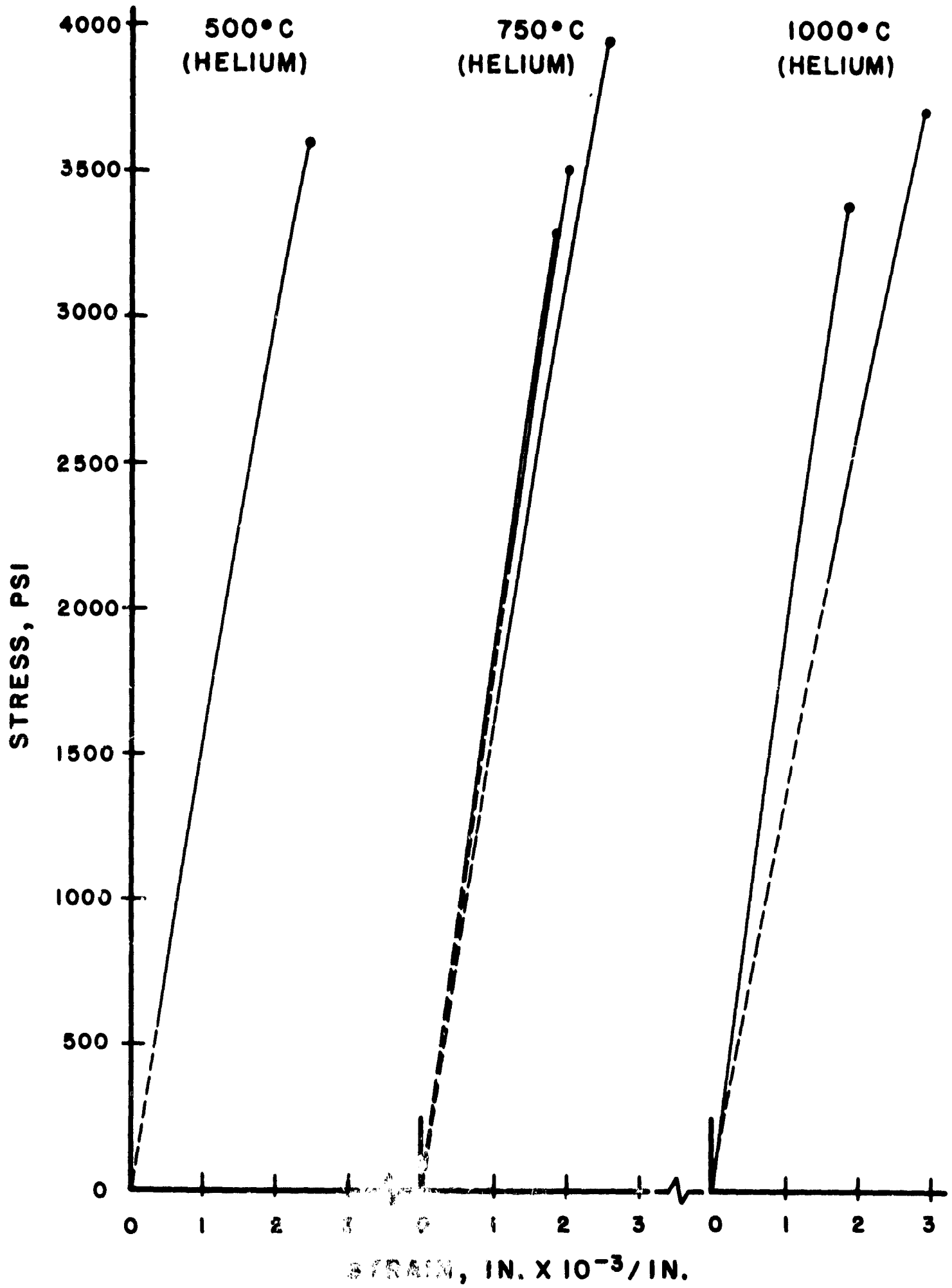
500° C
(HELIUM)
750° C
(HELIUM)
1000° C
(HELIUM)
4000
3500
3000
2500
2000
1500
1000
500
0
STRESS, PSI
0
1
2
3
0
1
2
3
0
1
2
3
STRAIN, IN. X 10⁻³/IN.

Figure C-2.

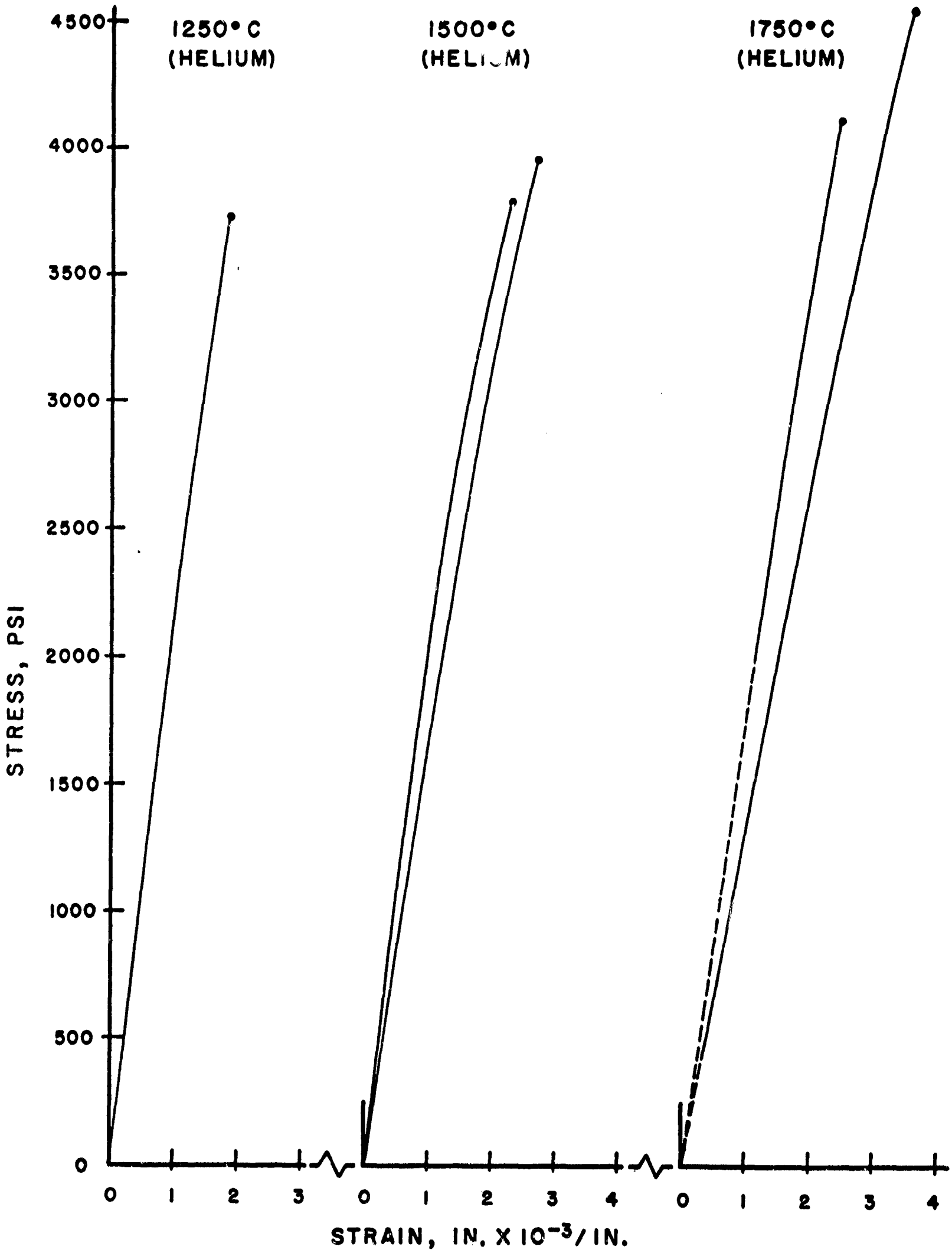
1250° C
(HELIUM)
1500° C
(HELIUM)
1750° C
(HELIUM)
4500
4000
3500
3000
2500
2000
1500
1000
500
0
STRESS, PSI
0 1 2 3
0 1 2 3 4
0 1 2 3 4
STRAIN, IN. X 10⁻³/IN.

Figure C-3.

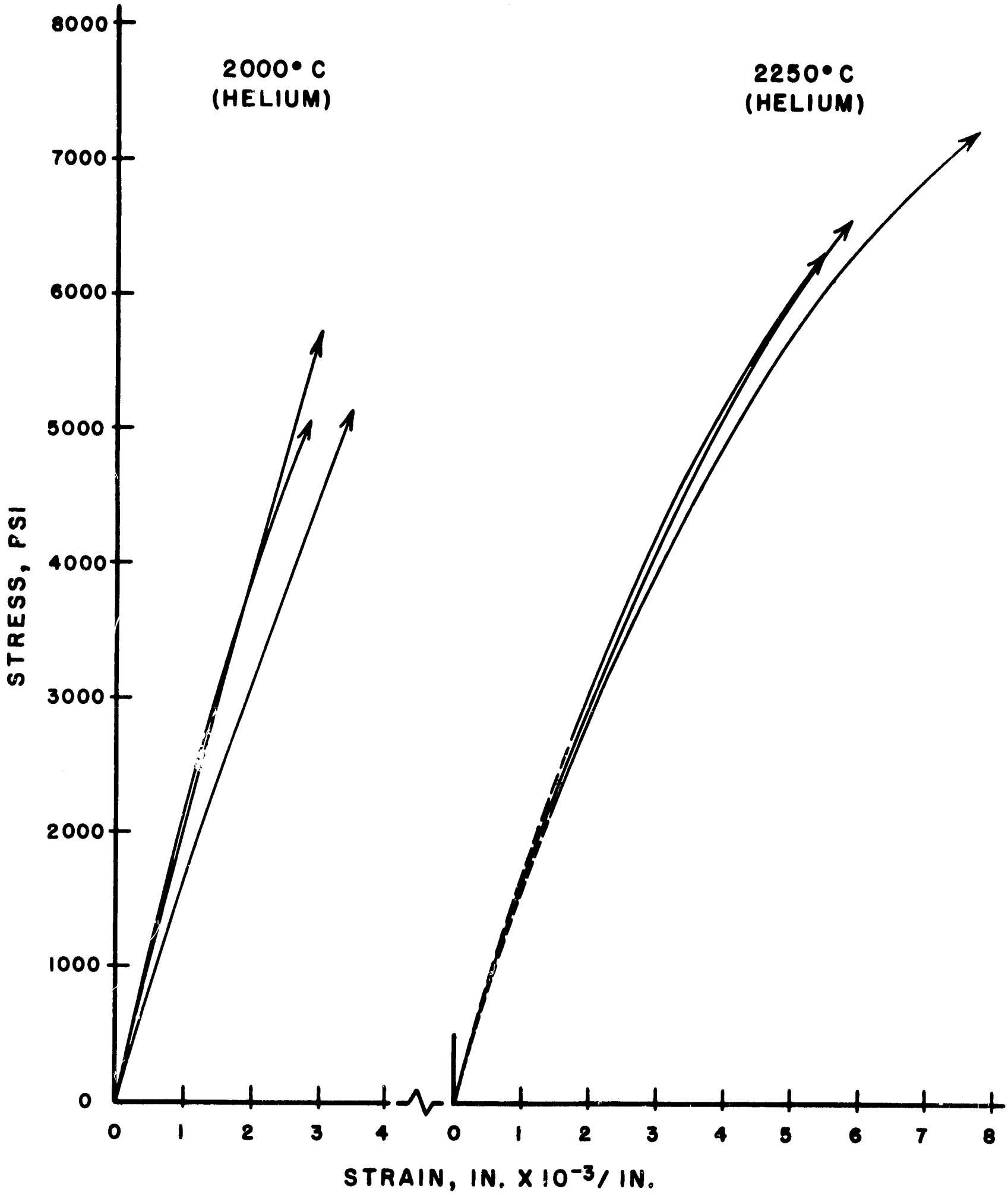
2000° C
(HELIUM)
2250° C
(HELIUM)
STRESS, PSI
8000
7000
6000
5000
4000
3000
2000
1000
0
0 1 2 3 4 0 1 2 3 4 5 6 7 8
STRAIN, IN. X 10⁻³/ IN.

Figure C-4.

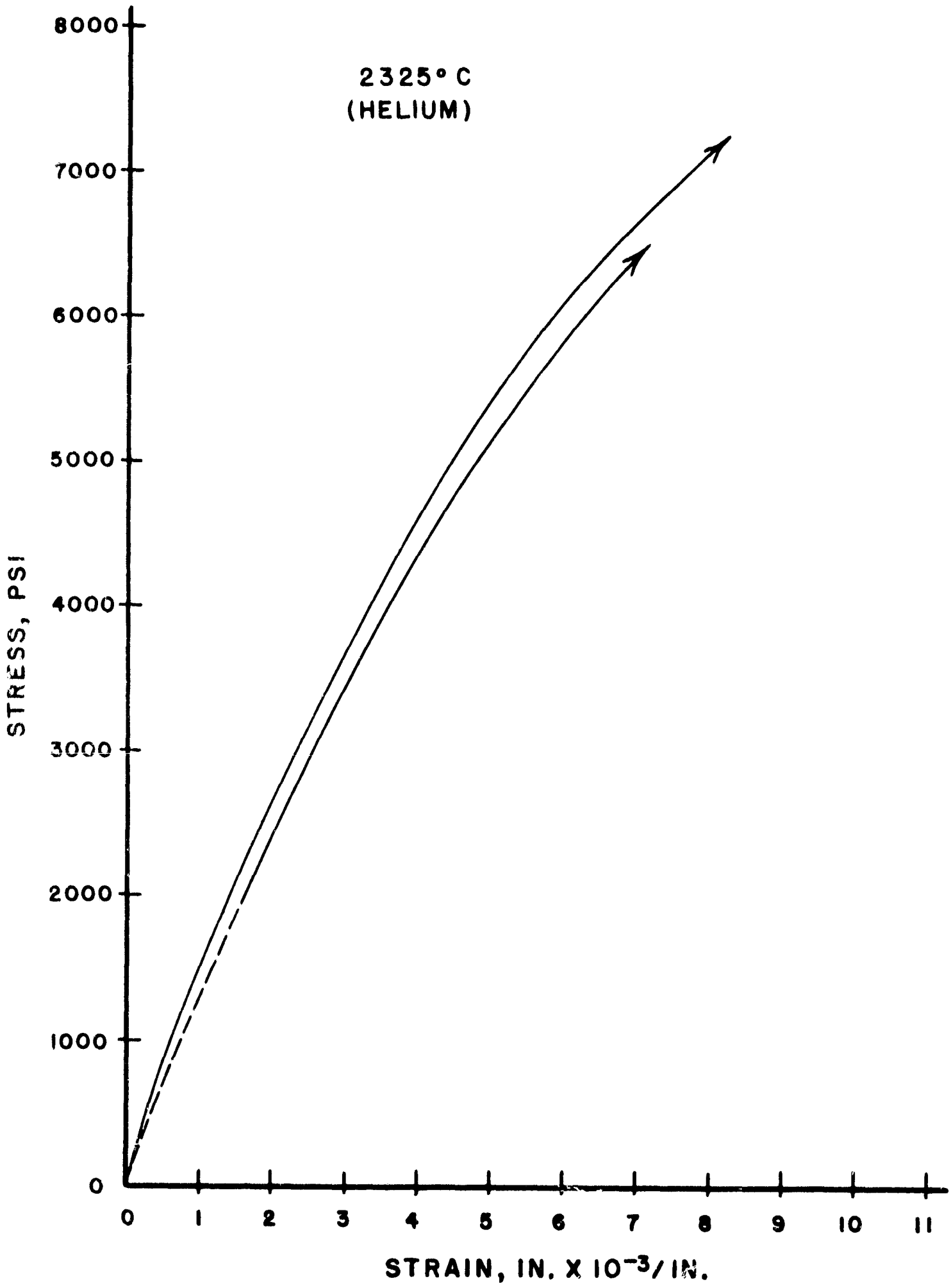
2325° C
(HELIUM)
8000
7000
6000
5000
4000
3000
2000
1000
0
STRESS, PSI
0
1
2
3
4
5
6
7
8
9
10
11
STRAIN, IN. X 10⁻³/IN.

Figure C-5.

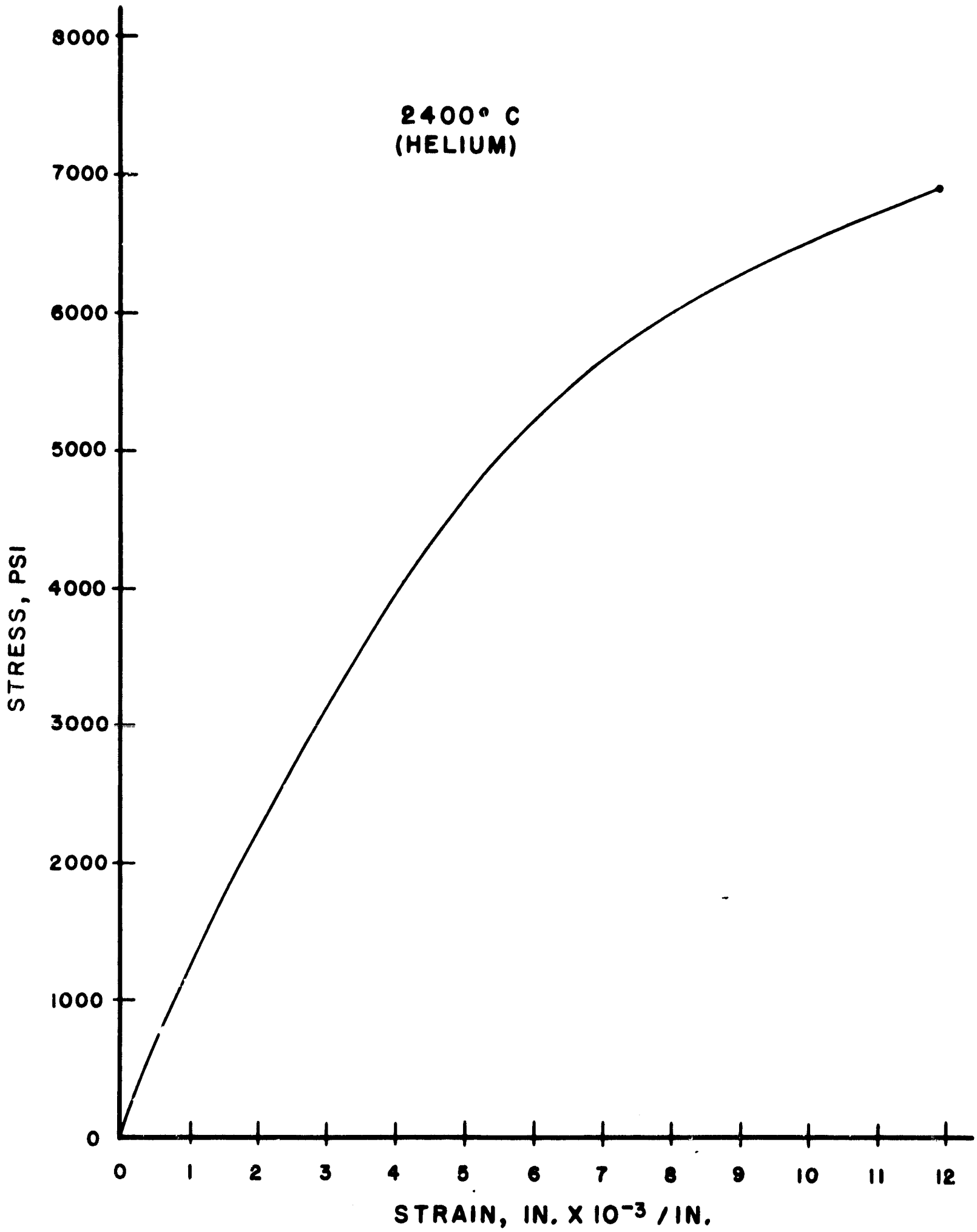
2400° C
(HELIUM)
STRESS, PSI
8000
7000
6000
5000
4000
3000
2000
1000
0
0
1
2
3
4
5
6
7
8
9
10
11
12
STRAIN, IN. X 10⁻³ / IN.

Figure C-6.

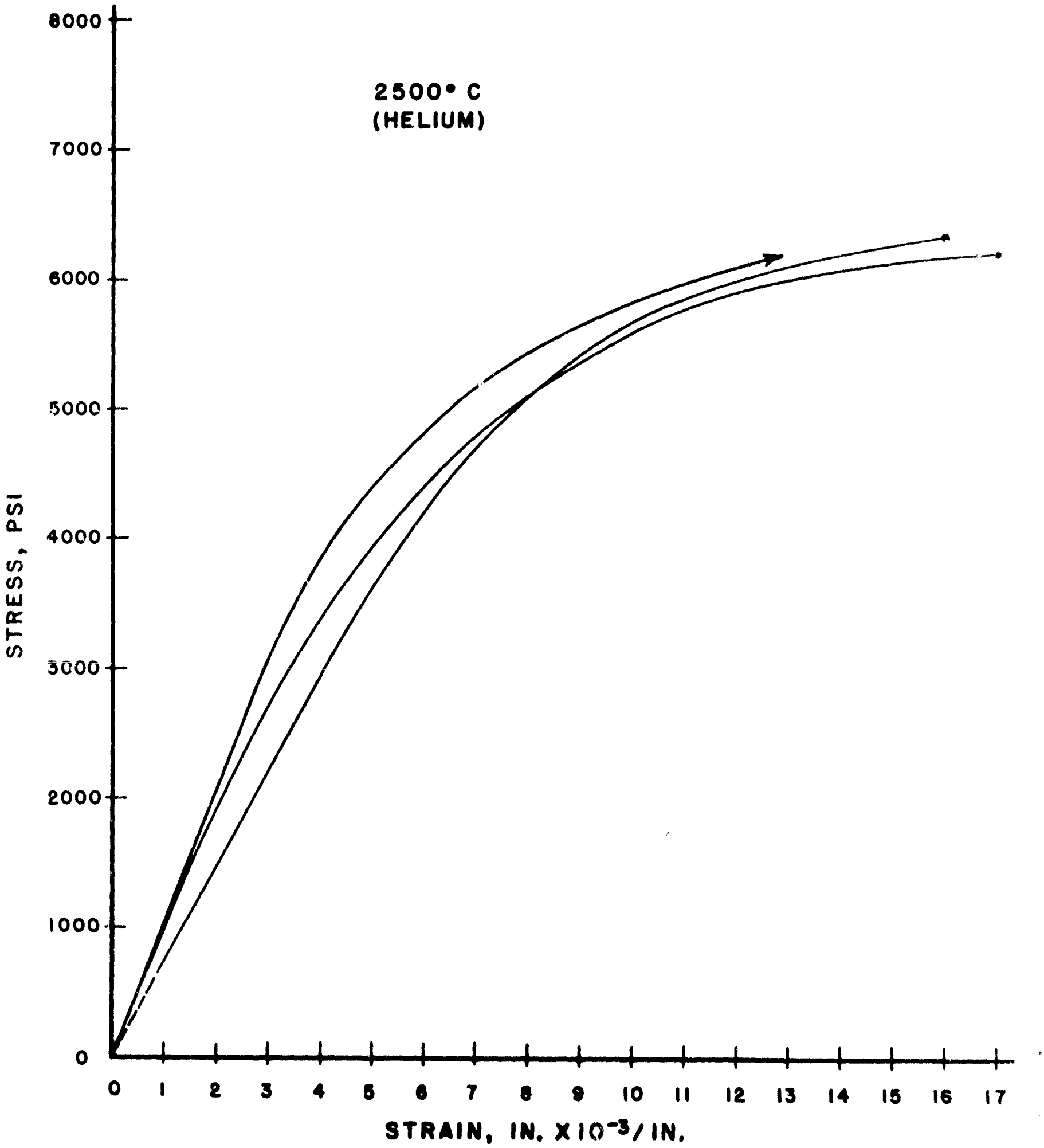
2500° C
(HELIUM)
STRESS, PSI
8000
7000
6000
5000
4000
3000
2000
1000
0
0 1 2 3 4 5 6 7 8 9 10 11 12 13 14 15 16 17
STRAIN, IN. X 10⁻³/ IN.

Figure C-7.

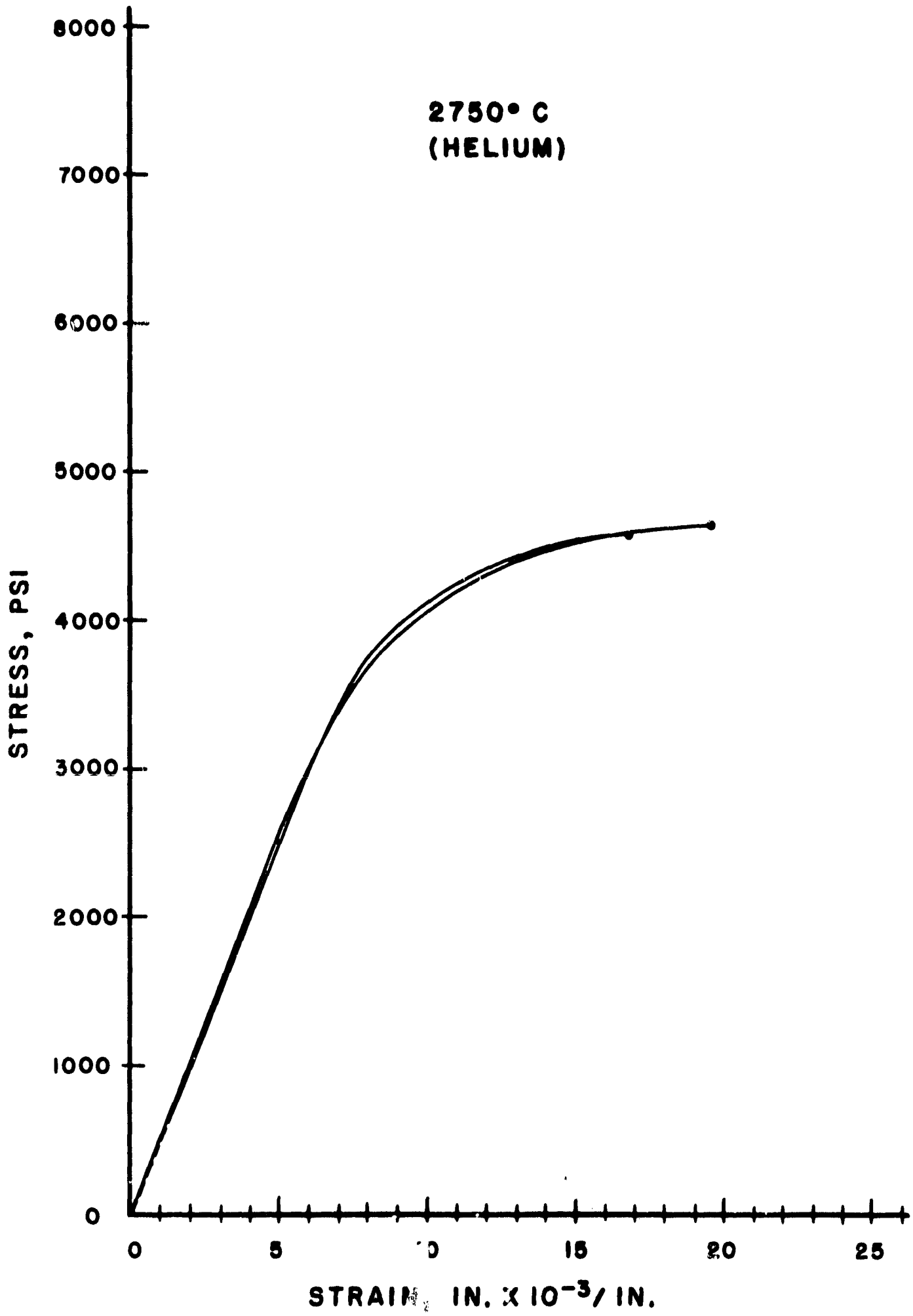
2750° C
(HELIUM)
8000
7000
6000
5000
4000
3000
2000
1000
0
STRESS, PSI
0
5
10
15
20
25
STRAIN, IN. X 10⁻³/ IN.

Figure C-8.